The Significance of the Leaf-Area-Index on the Evapotranspiration Estimation in SWAT-T for Characteristic Land Cover Types of Western Africa

Fabian Merk[1], Timo Schaffhauser[1], Faizan Anwar[1], Ye Tuo[1], Jean-Martial Cohard[2], and Markus Disse[1]

[1]School of Engineering and Design, Technical University of Munich, Munich. Germany
[2]Institute of Engineering and Management, University of Grenoble Alpes, Grenobles, France

Correspondence: Fabian Merk (fabian.merk@tum.de)

Abstract.

Evapotranspiration (ET) is pivotal in the terrestrial water cycle in sub-humid and tropical regions. In this, the contribution of plant transpiration can be distinctively more significant than soil evaporation. The seasonal dynamics of plant phenology, e.g., commonly represented as the vegetation attribute leaf-area-index (LAI), closely correlates with actual ET (AET). Hence, addressing the reciprocal LAI-AET interaction is essential for practitioners and researchers to comprehensively quantify the hydrological processes in water resources management, particularly in the perennially vegetated regions of Western Africa. However, due to the lack of field measurements, the evaluation of the LAI-AET interaction still remains challenging. Hence, our study aims to improve the understanding of the role of LAI on the AET estimation by investigating characteristic regions of Western Africa. We setup eco-hydrological models (SWAT-T) for two homogeneous land cover types (forest and grassland) to guarantee the representativeness of field measurements for LAI and AET. We apply different potential ET methods (Hargreaves, Penman-Monteith (PET-PM), Priestley-Taylor) to evaluate the LAI-AET interaction in SWAT-T. Further, the elementary effects method quantifies the parameter sensitivity for 27 relevant LAI-AET parameters. The comprehensive parameter set is then optimized using the Shuffled-Complex-Evolution algorithm. Finally, we apply a benchmark test to assess the performance of SWAT-T to simulate AET and to determine the relevance of a detailed LAI modeling. The results show that SWAT-T is capable of accurately predicting LAI and AET on the footprint scale. While all three PET methods facilitate adequate modeling of LAI and AET, PET-PM outperforms the methods for AET independent of the land cover type. Moreover, the benchmarking highlights that if an optimization process only accounts for LAI but disregards AET data, its prediction of AET still yields an adequate performance with SWAT-T for all PET methods and land cover types. Our findings demonstrate that the significance of detailed LAI modeling on the AET estimation is more pronounced in the forested than in the grassland region.

1 Introduction

Evapotranspiration (ET) is a key hydrological process of the continental water cycle, particularly in the sub-humid and tropical regions of Western Africa where the share of ET to precipitation can be up to 70 – 80 % (Rodell et al., 2015). The high share of ET in the water cycle inevitably necessitates the reliable estimation of ET for water resources studies on all scales in sub-humid

and tropical regions. Concurrently, the accurate computation of ET remains challenging for researchers and practitioners since ET is dynamic in space and time (Michel et al., 2016; Miralles et al., 2016). Its variability notably depends on land cover, soil properties, water availability, vegetation state, and time of the year (Chu et al., 2021). In addition, plant transpiration has a decisive contribution to the total evapotranspiration (Gerten et al., 2004; Schlesinger and Jasechko, 2014; Miralles et al., 2016; Wei et al., 2017). It is directly linked to the canopy conductance, which strongly correlates with the leaf-area-index (LAI) (Good et al., 2014; Wang et al., 2014). Thus, in perennially vegetated regions with high transpiration rates, such as sub-humid Western Africa, the LAI-ET interaction plays a pivotal role in the ET quantification (Schlesinger and Jasechko, 2014; Wei et al., 2017; Bright et al., 2022).

Although important, the availability of LAI and ET ground measurements is scarce. In previous ET studies, authors have used existing global monitoring networks, such as eddy covariance (EC) systems (e.g., AmeriFlux (Novick et al., 2018), AMMA-CATCH (Galle et al., 2018), or FLUXNET (Friend et al., 2007)), to inform catchment-scale hydrological models to comprehensively assess all processes of the hydrological cycle (Schneider et al., 2007; Hector et al., 2018; Ferreira et al., 2021; Jepsen et al., 2021; López-Ramírez et al., 2021). Still, the derived AET estimates from EC systems can not be extrapolated without limitations beyond the location site. This is mainly attributed to the small footprint, i.e., the source area of the AET fluxes. Depending on soil and land cover properties underlying the footprints, the source area spatially limits the representativeness of the AET measurements (Chu et al., 2021). For LAI, the limited availability of field observations is commonly addressed by exploiting satellite-based LAI data. A favorable data set is thereby the Global Land Surface Satellite (GLASS) LAI data (Liang et al., 2021) where the widely used MODIS LAI data has been advanced with machine learning applications on the global scale (Liang et al., 2014). The validation reports of GLASS-LAI data present accurate LAI time series results, particularly in perennially vegetated regions (Liang et al., 2014) where the satellite-based vegetation data can be subject to noise and cloud influences (Viovy et al., 1992; Strauch and Volk, 2013; Atkinson et al., 2012; Alemayehu et al., 2017).

In the present study, the semi-distributed, physically-based eco-hydrological Soil and Water Assessment Tool for the tropics (SWAT-T) (Alemayehu et al., 2017) is applied. The SWAT-T model is a modification of SWAT (Arnold et al., 1998), which has been introduced by Strauch and Volk (2013) and further developed by Alemayehu et al. (2017) to account for a more realistic plant growth modeling of perennial vegetation in tropical regions. The merits of SWAT-T for an improved prediction of LAI and AET have been highlighted in different tropical and sub-humid regions. It has been applied on the catchment scale in Eastern Africa (Alemayehu et al., 2017), in Colombia (Hoyos et al., 2019), in Brazil (Ferreira et al., 2021) as well as in Australia (Zhang et al., 2020) and on the micro-catchment scale in Mexico (López-Ramírez et al., 2021). Moreover, the application of SWAT-T for climate impact assessment has been presented in Peru on the catchment scale (Fernandez-Palomino et al., 2021). Remotely-sensed AET has been chiefly employed to assess the model fitness of simulated AET with SWAT-T (Alemayehu et al., 2017; Zhang et al., 2020; Fernandez-Palomino et al., 2021; Ferreira et al., 2021) as well as with SWAT (Rajib et al., 2018; Qiao et al., 2022). The latest, open-source version of SWAT, called SWAT+, has also been applied in the tropics with remotely-sensed AET and LAI data (Abitew et al., 2023). For the African continent, remotely-sensed AET products can be limited due to uncertainties in their reliability (Weerasinghe et al., 2020).

For the LAI estimation, the SWAT-T studies mentioned above relied on the application of remotely-sensed LAI from MODIS. In the past, measured LAI was used with SWAT (Park et al., 2017; Yang et al., 2018; Nantasaksiri et al., 2021; Haas et al., 2022) as well as observed forest biomass production (Khanal and Parajuli, 2014; Haas et al., 2022) for an analysis of the LAI model parameters. The number of LAI parameters thereby differ from three (Yang et al., 2018) to 18 (**?**) parameters. For tropical regions, Alemayehu et al. (2017) suggests the calibration of 11 LAI parameters when SWAT-T is applied. LAI and AET are correlated and influence each other in SWAT/SWAT-T (Arnold et al., 1998). For example, the water stress on plants is dependent on AET and can determine the actual plant growth in SWAT/SWAT-T (Neitsch et al., 2011). When modeling LAI, the relevant AET parameters must therefore be considered.

To the best of our knowledge, the integration of measured LAI and AET data in the evaluation of the reciprocal LAI-AET interaction and the relevance of a coupled LAI-AET parameter estimation with the SWAT/SWAT-T model has yet to be considered. Previous studies on the influence of LAI on AET in SWAT/SWAT-T have either not covered all relevant LAI-AET parameters, considered only heterogeneous source areas of measured AET, or only used remotely sensed AET and LAI data. Hence, we address these shortcomings and focus on the comprehensive evaluation of the significance of LAI on AET in SWAT-T with measured LAI and AET data. Further, we test the hypothesis of whether a detailed plant growth model optimization (single LAI optimization regarding observed or GLASS-LAI) can still adequately estimate AET with SWAT-T.

We evaluate the LAI-AET interaction for two typical, perennially vegetated land cover types of Western Africa using a SWAT-T model on the seamless footprint scale of the EC system for each site. The sites are located in the sub-humid Bétérou catchment in Benin. First, we highlight the relevance of a coupled LAI-AET parameter estimation of predicting LAI. Then, a global sensitivity analysis using the elementary effects method (Morris, 1991) is applied to quantify the parameter sensitivities and to enable a ranking of the sensitivity levels. We optimize the LAI-AET parameters with LAI data (observed and GLASS-LAI), exclude AET as a proxy in the model optimization, and eventually evaluate the AET model response of the LAI optimization. For this purpose, the performance test proposed by Seibert et al. (2018) is conducted. The test compares the best-optimized model (simultaneous LAI and AET optimization as upper benchmark) with single LAI optimization approaches (observed or GLASS-LAI). To provide a lower limit of the general LAI-AET performance of SWAT-T, a random sampling approach of the LAI-AET parameters (lower benchmark) is applied. The LAI-AET parameter optimization is conducted using the Shuffled-Complex-Algorithm (SCE-UA) (Duan et al., 1994).

2 Methods

Figure 1 gives an overview of the methods applied in this study to evaluate the significance of LAI on the AET estimation in SWAT-T. First, the input data is processed and footprint scales SWAT-T models for two characteristic, perennially vegetated regions in Western Africa are setup. Second, the relevance of a coupled LAI-AET parameter estimation is investigated with one-at-a-time parameter changes and evaluated regarding observed LAI and AET data. Third, the sensitivity analysis is conducted based on the elementary effects method concerning observed LAI. Finally, the role of LAI on the AET estimation in SWAT-T

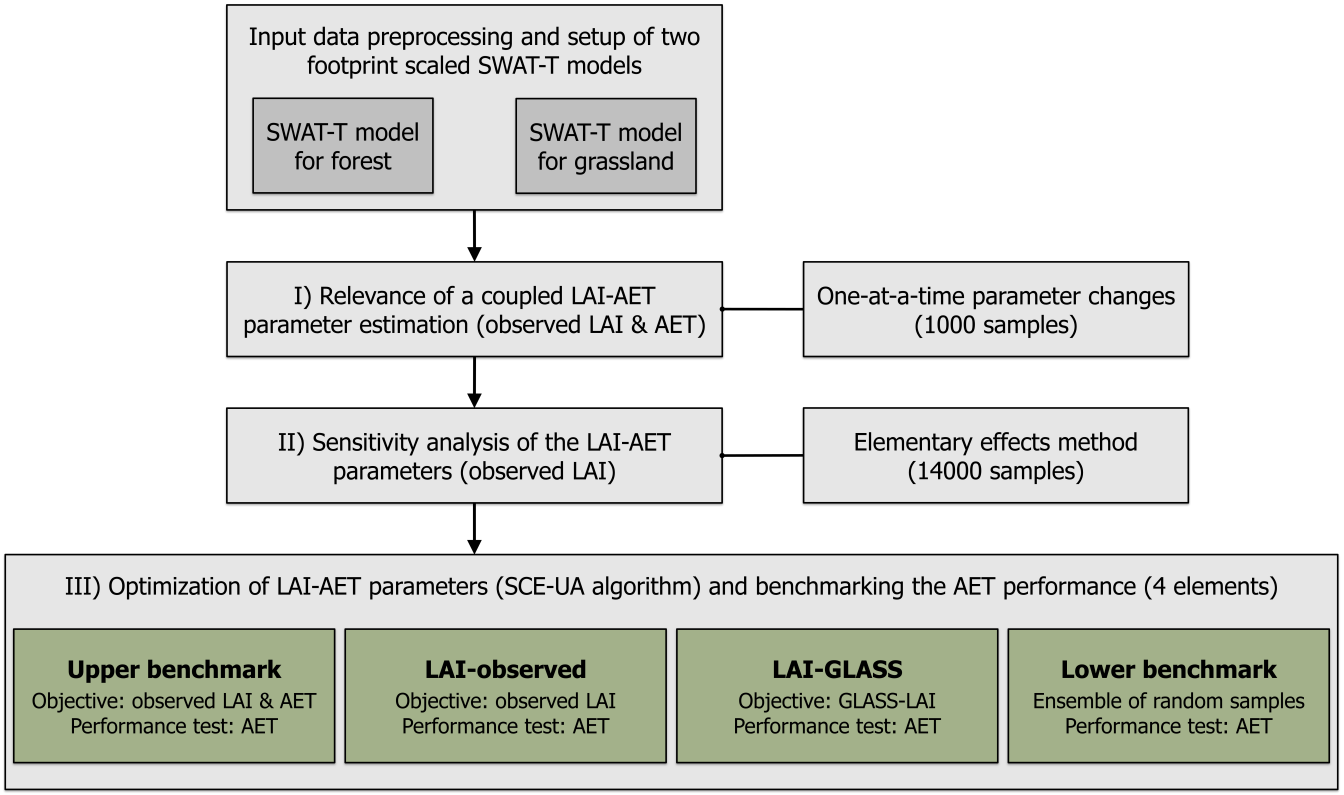

Figure 1. Methods to assess the significance of LAI on AET estimation as applied in the present study. Three different PET methods (Hargreaves, Priestley-Taylor, Penman-Monteith) available in SWAT-T are applied for all three steps of the methodology.

is assessed with an optimization approach (Shuffled-Complex-Evolution algorithm) and the performance of predicting AET is tested with a benchmark test.

2.1 Model description and parameter selection

The SWAT-T model is an enhanced version of the ecohydrological model SWAT (Arnold et al., 1998). In SWAT-T, the plant growth module has been modified to account for a more realistic perennial plant phenology in tropical regions (Alemayehu et al., 2017) which can improve the AET prediction (Zhang et al., 2020; Fernandez-Palomino et al., 2021; Ferreira et al., 2021; López-Ramírez et al., 2021). Apart from the plant growth module, SWAT-T and SWAT are identical. The original SWAT model has been applied worldwide in different river basins (Arnold and Fohrer, 2005; Tan et al., 2020) and regionally in Benin (Akoko et al., 2021). Specifically in Benin, most of the applications focused on the discharge assessment for the Ouémé river basin (Bossa et al., 2014; Poméon et al., 2018) and its tributaries (Giertz et al., 2006; Bossa et al., 2012; Duku et al., 2016, 2018; Danvi et al., 2017; Togbévi et al., 2020). In previous studies in Western Africa, remotely-sensed AET was also used as a main

calibration objective to predict streamflow (Odusanya et al., 2019, 2021). To the best of our knowledge, the SWAT-T model has not been applied in Benin but in Eastern Africa (Alemayehu et al., 2017).

The SWAT/SWAT-T model is generally spatially discretized into subbasins and subdivided into hydrological response units (HRUs). Three options are available to compute the potential ET (PET) in SWAT/SWAT-T: the temperature-based Hargreaves (PET-HG) (Hargreaves and Samani, 1985), the energy-based Priestley-Taylor (PET-PT) (Priestley and Taylor, 1972) and the combined temperature and energy-based Penman-Monteith (PET-PM) (Monteith, 1965) method. Table 1 summarizes the equations for how PET E_0 is computed and highlights the integral part of LAI in each approach.

Table 1. Approaches to compute potential evapotranspiration E_0 and potential transpiration T_{plant} provided in SWAT-T.

PET method	Equation for E_0	Equation for T_{plant}
PET-HG	$E_0 = \frac{0.0023 \cdot H_0}{\lambda} \cdot \sqrt{T_{mx} - T_{mn}} \cdot (T_{av} + 17.8)$	$T_{plant} = \begin{cases} LAI \cdot \frac{E_0}{3.0}, & \text{if } LAI \leq 3.0 \\ E_0, & \text{if } LAI > 3.0 \end{cases}$
PET-PT	$E_0 = \frac{\alpha_{pet} \cdot \Delta}{\lambda \cdot (\Delta + \gamma)} \cdot (H_{net} - G)$	$T_{plant} = \begin{cases} LAI \cdot \frac{E_0}{3.0}, & \text{if } LAI \leq 3.0 \\ E_0, & \text{if } LAI > 3.0 \end{cases}$
PET-PM	$E_0 = \frac{\Delta \cdot (H_{net} - G) + \rho_{air} \cdot c_p \cdot (e_z^0 - e_z)/r_a}{\lambda \cdot (\Delta + \gamma \cdot (1 + r_c/r_a))},$ with r_c, r_a from alfalfa crop reference	$T_{plant} = \frac{\Delta \cdot (H_{net} - G) + \rho_{air} \cdot c_p \cdot (e_z^0 - e_z)/r_a}{\lambda \cdot (\Delta + \gamma \cdot (1 + r_c/r_a))},$ with r_c, r_a from actual plant (canopy height and LAI)

In the equations in Table 1 λ is the latent heat of vaporization, H_0 is the extraterrestrial radiation, T_{mx}, T_{mn}, and T_{av} are the maximal, minimal, and mean daily temperature, respectively, α_{pet} is a coefficient, Δ is the slope of the saturation vapor pressure-temperature, γ is the psychcrometric constant, H_{net} is the net radiation, G is the heat flux density to the ground, ρ_{air} is the air density, c_p is the specific heat at constant pressure, e_z^0 is the saturation vapor pressure of air at height z, e_z is the water vapor pressure of air at height z, r_a is the aerodynamic resistance, and r_c is the plant canopy resistance. In PET-PM, r_a and r_c are attributed to the alfalfa crop reference for the computation of E_0 (Neitsch et al., 2011). After the calculation of E_0, it is partitioned into potential plant transpiration T_{plant} and soil evaporation E_{soil}. T_{plant} is thereby computed depending on the values of LAI for the given day for all PET methods. For PET-HG and PET-PT, a threshold of $LAI = 3.0$ determines if T_{plant} is equal to E_0, i.e., all potential evapotranspiration is coming only from the plant transpiration without the consideration of soil evaporation. If $LAI \leq 3.0$, a share of E_0 is potentially available for T_{plant} and E_{soil}. For PET-PM, T_{plant} is computed using the equation of Penman-Monteith (Table. 1) where r_a and $_c$ are determined concerning the modeled plant canopy and LAI.

E_{soil} for PET-PM is then $E_{soil} = E_0 - T_{plant}$. The actual plant transpiration and soil evaporation are computed depending on the water availability and different biophysical parameters, such as LAI or root depth, and soil properties, such as the field capacity. Actual plant transpiration and soil evaporation are then summed to the actual ET (AET).

The plant growth computation in SWAT/SWAT-T follows the approach of the "Environmental Policy Impact Climate" (EPIC) model (Arnold et al., 1998) where LAI is a key vegetation attribute for the plant phenology (Neitsch et al., 2011). Generally, the plant growth in SWAT/SWAT-T can be divided into an initial phase (start of the growing phase), a growing phase, a period of maturity (growing is halted to a constant LAI), the leaf senescence phase (natural decline of the plant and a decreasing LAI), and a dormancy period (no plant growth but constant LAI). In the growing phase, the optimal leaf development in SWAT/SWAT-T is computed with:

$$fr_{LAI_{mx}} = \frac{fr_{PHU}}{fr_{PHU} + exp(l_1 - l_2 \cdot fr_{PHU})}, \tag{1}$$

where $fr_{LAI_{mx}}$ is the fraction of the maximum leaf area index of a plant with respect to the fraction of the potential heat units for the plant, fr_{PHU} is the fraction of the potential heat units in the current day of the growth cycle, and l_1 and l_2 are shape coefficients. The plant growth continues until the maximum leaf area index is reached:

$$\Delta LAI_i = (fr_{LAI_{mx},i} - fr_{LAI_{mx},i-1}) \cdot LAI_{mx} \cdot (1 - exp(5 \cdot (LAI_{i-1} - LAI_{mx}))), \tag{2}$$

For perennial plants, the LAI for the given day i under optimal conditions is computed as:

$$LAI_i = LAI_{i-1} + \Delta LAI_i. \tag{3}$$

However, the optimal plant growth can be constrained in SWAT/SWAT-T due to water, temperature, nitrogen, or phosphorous stress. The water stress $wstrs$ is thereby directly linked to the actual plant transpiration and the total water plant uptake. The temperature stress $tstrs$ is computed based on the air temperature of the given day and the user-defined parameters T_{base} and T_{opt}. Nitrogen and phosphorus stresses, $nstrs$ and $pstrs$, respectively, are computed to account for insufficient nutrients (see Appendix A2 for the supplementary equations). The actual plant growth is determined with a plant growth factor γ_{reg}:

$$\gamma_{reg} = 1 - max(wstrs, tstrs, nstrs, pstrs), \tag{4}$$

and the actual leaf area added on a day i is computed as:

$$\Delta LAI_{act,i} = \Delta LAI_i \cdot \gamma_{reg}. \tag{5}$$

The major difference between the plant growth modeling in SWAT and SWAT-T are two features: the logarithmic decline of LAI and the automatic start of the growing phase based on a soil moisture index. In the first plant growth modification of SWAT, Strauch and Volk (2013) introduced a logarithmic decline of LAI in the leaf senescence phase for a more realistic representation of the LAI decrease and to avoid a rapid drop of LAI:

$$LAI = \frac{LAI_{max} - LAI_{min}}{1 + exp(-t)}, \tag{6}$$

where t is defined considering the fraction of the potential heat units at which senescence become the dominant growth phase $fr_{PHU_{sen}}$ as:

$$t = 12 \cdot \left(\frac{1 - fr_{PHU}}{1 - fr_{PHU_{sen}}} - 0.5 \right) \text{ if } fr_{PHU} \geq fr_{PHU_{sen}}. \quad (7)$$

Since plant growth in the tropics is generally governed by the water availability in the soils (Jolly and Running, 2004), Alemayehu et al. (2017) further modified the SWAT version of Strauch and Volk (2013) and implemented an automatic start of the growing phase which is triggered by the soil moisture index. For this purpose, the soil moisture index $SMI = P/E_0$ is introduced. The precipitation P is aggregated for a user-defined time window (here: 5 days). A SMI threshold to start the growing has to be defined (here: $SMI = 0.5$). To avoid false starts of the new growing cycle, the end of the dry season (SOS_1, here: October) and the beginning of the rainy season (SOS_2, here: January) have to be specified by the user, too (Alemayehu et al., 2017). In SWAT, the start of the growing phase is linked to the number of accumulated heat units. In SWAT-T, the soil moisture index has replaced this dependency of the heat units. The heat units are mainly used in SWAT-T to define the plant growth development over the year (see Equ. 1).

27 parameters have been selected to investigate the LAI-AET interaction (Table 2). The selection of LAI parameters follows the suggestion of Alemayehu et al. (2017), whereas the AET parameters are chosen based on literature review. In the past, 27 parameters of SWAT were assessed for sensitivity analysis with a particular focus on AET (Ha et al., 2018; Odusanya et al., 2019; Bennour et al., 2022; Koltsida and Kallioras, 2022). Parameters with a coinciding low sensitivity reported in these studies, e.g., the hydraulic conductivity in the channel (CH_K2) or groundwater baseflow delay (GW_DELAY), are not considered in the present LAI-AET parameter list to reduce the total parameter space. For the present study, the soil layer thickness (SOL_D) is given for four soil layers from field measurements (Judex and Thamm, 2008). We adjust only the depth of the lowest soil layer to not excessively shape the ground-truth observations but to still facilitate an evaluation of the influence of the total soil thickness on the LAI-AET interaction in SWAT-T.

2.2 Study site and footprint-scaled models

The study sites Bellefoungou and Naholou are located in the Western part of the Bétérou catchment (Figure 2). The climate is typical for Sub-Saharan, sub-humid Africa. The annual precipitation ranges from 1100 to 1500 mm (Mamadou et al., 2016; Bliefernicht et al., 2019). The precipitation pattern is unimodal, with a rainy season between April and October, whereas from November to March, the dry season occurs. The annual mean daily temperature is 25°C (Galle et al., 2018). The soils in the Bétérou catchment consist of ferric soils with loamy sand present in the upper soil horizons (Giertz and Diekkrüger, 2003). Generally, the AET data follows the seasonality of LAI (Figure 2). Still, a decrease in AET in the wet season can be observed for this region. AET depends on radiation, wind speed, and humidity. The net radiation decreases during the wet season, automatically reducing fluxes like sensible and latent heat fluxes (cf. A1). Additionally, the atmospheric demand is reduced because of high air humidity, which was observed for the vapor pressure deficit (Mamadou et al., 2016) resulting in lower AET rates in the wet season.

Table 2. List of parameters used to estimate LAI and AET with their description.

Parameter	Description [unit]
Parameters associated with plant growth (LAI) in the plant data base of SWAT	
BIO_E	Radiation-use efficiency [(kg/ha)/(MJ/m^2)]
BLAI	Maximum potential leaf area index [m^2/m^2]
$FRGRW_1$	Fraction of PHU corresponding to the first point on the optimal leaf area development curve [-]
$LAIMX_1$	Fraction of BLAI corresponding to the first point on the optimal leaf area development curve [-]
$FRGRW_2$	Fraction of PHU corresponding to the second point on the optimal leaf area development curve [-]
$LAIMX_2$	Fraction of BLAI corresponding to the second point on the optimal leaf area development curve [-]
DLAI	Fraction of total PHU when leaf area begins to decline [-]
T_OPT	Optimal temperature for plant growth [°C]
T_BASE	Minimum temperature for plant growth [°C]
ALAI_MIN	Minimum leaf area index for plant during dormant period [m^2/m^2]
PHU	Total number of heat units needed to bring plant to maturity [-]
GSI	Maximum stomatal conductance [m/s]
Parameters associated with AET estimation	
CAN_MX	Maximum canopy storage [mm]
ESCO	Soil evaporation compensation factor [-]
EPCO	Plant uptake compensation factor [-]
HRU_SLP	Average slope steepness [m/m]
SLSUBBSN	Average slope length [m]
CN2	Initial SCS runoff curve number [-]
SOL_AWC	Available water capacity of the soil layer [mm]
SOL_BD	Moist bulk density [g/cm^3]
SOL_CBN	Organic carbon content [% soil weight]
SOL_K	Saturated hydraulic conductivity [mm/hr]
SOL_RD	Maximum rooting depth of soil profile [mm]
SOL_D[a]	Soil layer depth [mm]
GW_REVAP	Groundwater re-evaporation coefficient [-]
RCHRG_DP	Deep aquifer percolation fraction [-]
REVAPMN	Threshold depth of water for re-evaporation to occur [mm]

[a]Here: lowest soil layer depth

The forested Bellefoungou region (latitude 9.791°N, longitude 1.718°E, 445 masl) is covered with typical, widespread woodland ("clear forest") for Sub-Saharan Africa (Ago et al., 2016). The Naholou region (latitude 9.74°N, longitude 1.60°E, 449 masl) is covered mainly by a characteristic mixture of crops and savannah grassland and fallows (Ago et al., 2014). Due to the high share of grassland, the Naholou region is hence defined as a grassland region in the following. The estimated flux

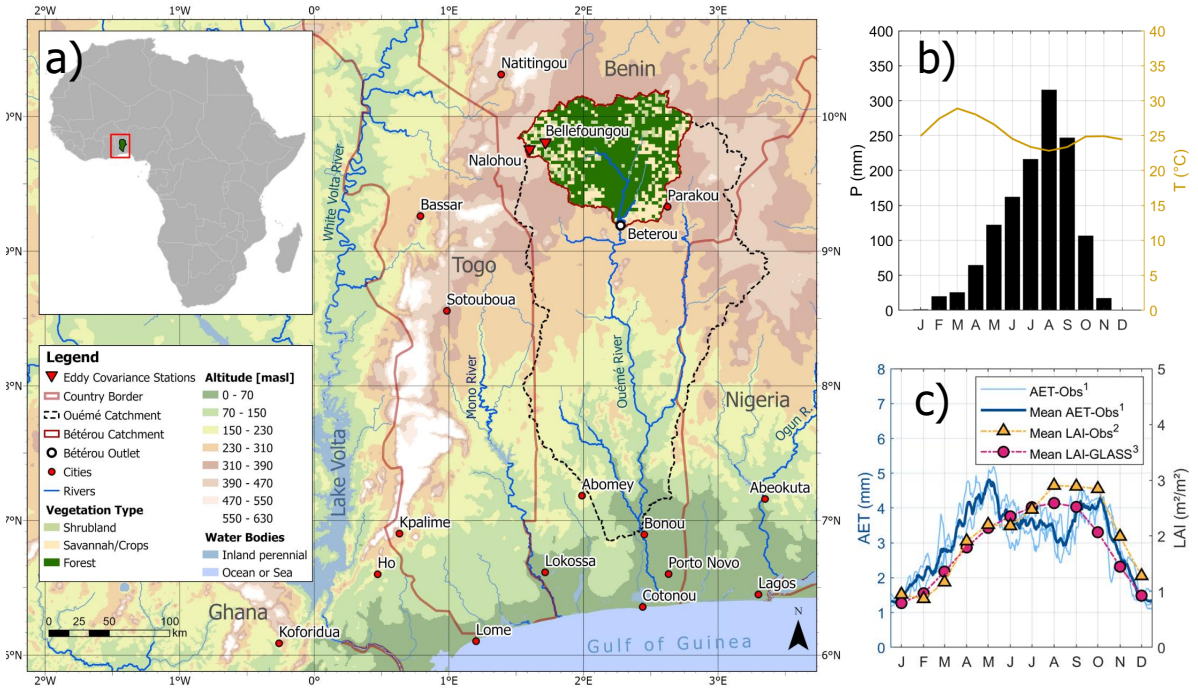

Figure 2. a) Overview of the Bétérou catchment and the locations of the eddy covariance systems (Naholou and Bellefoungou); b) the seasonality of precipitation and temperature in Bellefoungou; c) and the comparison of observed AET (in blue), mean monthly values for observed LAI (yellow), and mean monthly values for GLASS-LAI (in purple) in Bellefoungou. The solar radiation, wind speed, and relative humidity for the sites are illustrated in the appendix (cf. A1). References for the data used to display the map are listed in the appendix (cf. A5). The superscripts in c) denote the corresponding time periods: [1]from 01/2008 to 12/2010; [2]from 07/2008 to 05/2010; [3]from 01/2007 to 12/2015.

footprint extent for the grassland region is 4000 m^2, while for the forested region, it is seasonally varying and can be up to 60000 m^2 (Mamadou et al., 2014). AET accounts for high shares of precipitation at both sites where the share of annual AET to precipitation is 57 % and 72 % for Naholou and Bellefoungou, respectively (Mamadou et al., 2016). The evaporative fraction (share of plant transpiration to total AET) is exceptionally high in the wet season. The values for the evaporative fraction are 70 ±2.5 % at Naholou and 75 ±0.7 % at Bellefoungou (Mamadou et al., 2016). These high plant transpiration rates to AET demonstrate the strong dependency of plant growth and AET in these regions (Mamadou et al., 2016; Hector et al., 2018). The field measurements for LAI in both sites were delineated from hemispherical photographs and the processing methodology proposed by Weiss et al. (2004). The in situ data is complemented with corrections of an ensemble of satellite-based LAI products (CYCLOPE, MODIS, SEVIRI) (Mamadou et al., 2014).

One SWAT-T model is set up for the forested and the grassland site in the Bétérou catchment, respectively. No footprint calculations for the sites or the necessary data to compute those are available. We thus adhere to the suggestion of Chu et al. (2021) where radii of $< 250\ m$ around flux towers assure flux representativeness. The SWAT/SWAT-T models are watershed

Table 3. Overview of the data sets that are applied in this study.

Variable	Resolution	Database name or source
Digital elevation model	Rastered DEM, 30 m x 30 m	Copernicus GLO-30 (Copernicus, 2022)
Soil map	Soil type clusters	IMPETUS Soil Map (Judex and Thamm, 2008)
Observed AET	Daily, pointwise	Mamadou et al. (2016)
Observed LAI	Daily, pointwise	Ago et al. (2014); Mamadou et al. (2016)
GLASS-LAI	Rastered, 250 m x 250 m	GLASS-LAI (Liang et al., 2021)
Precipitation	Daily, pointwise	AMMA-Catch network (Galle et al., 2018)
Temperature	Daily, pointwise	AMMA-Catch network (Galle et al., 2018)
Solar radiation	Daily, pointwise	AMMA-Catch network (Galle et al., 2018)
Relative humidity	Daily, pointwise	AMMA-Catch network (Galle et al., 2018)
Wind speed	Daily, pointwise	AMMA-Catch network (Galle et al., 2018)

models. For the model delineation with SWAT-T, we drew circles (250 m radius) around each flux tower to guarantee the representativeness of the flux footprints. Based on the underlying DEM, the resulting watershed extents are 8500 m^2 and 2300 m^2 for the forested and grassland sites, respectively. Although the footprint extent in the forested region can be larger depending on the season (Mamadou et al., 2016), we applied a constant extent following the suggestion of Chu et al. (2021). To ensure the homogeneity of land cover and soil properties, each SWAT-T model consists of a single HRU. LAI and AET are simulated on the daily time step. The data sets used in this study are listed in Table 3. The land cover type for each site (forest, grassland) represented in the model is provided in Ago et al. (2014, 2016). We defined the land use classes "FRSD" and "RNGE" from the SWAT crop database to the forested and grassland region, respectively. The observed AET data for both sites is available from 1/1/2008 to 31/12/2010 (Mamadou et al., 2016). The observed LAI data for the forested region (Bellefoungou) is available from 1/7/2008 to 31/5/2010 (Ago et al., 2016), for the grassland region (Naholou) from 5/8/2007 to 2/1/2010 (Ago et al., 2014). The meteorological data provided by the AMMA-Catch network dates from 2005 to 2020 (Galle et al., 2018). The GLASS-LAI data is provided from 2000 to 2021 (Liang et al., 2021). To enable the best possible overlap of measured LAI and AET data, the study periods from 1/1/2008 to 31/12/2010 and from 1/1/2007 to 31/12/2010 in the forested and grassland regions are defined, respectively.

2.3 Evaluation of the coupled LAI-AET parameter estimation

We postulate that for a comprehensive plant growth modeling in SWAT-T, the LAI and AET model parameters are decisive, particularly if the accurate estimation of plant transpiration is a modeling objective. We apply parameter changes and compare the corresponding model responses to observed AET and LAI to assess the relevance of a coupled LAI-AET parameter estimation. Each parameter from Table 2 is randomly sampled (1000 samples), and the model is run for each sample. In each simulation, the other model parameters remain unaltered (one-at-a-time parameter changes). To avoid influences from poorly estimated parameter values (e.g., the default settings), the optimized model parameters from the LAI-AET optimization (cf.

Section 2.5) are prescribed for the unaltered parameters. The model response of a parameter change is evaluated in two ways: with respect to observed AET and with respect to observed LAI. Finally, an evaluation of how LAI parameters influence the AET responses and how AET parameters influence the LAI responses is presented with this approach. The analysis of the LAI-AET parameter estimation is conducted for three PET methods (Hargreaves, Penman-Monteith, Priestley-Taylor) for the forested study site. The results for the grassland region are similar but not explicitly presented.

2.4 Sensitivity analysis with the Morris method

A sensitivity analysis for all LAI-AET parameters is conducted to address the parameter-response-complexity of the coupled LAI-AET modeling with SWAT-T. Sensitivity analysis is an essential yet challenging step in the application of hydrological models and the evaluation of reliable parameter sets, particularly with respect to model equifinality. Different approaches exist to quantify the model responses to parameter changes. In this study, we take advantage of the elementary effects method, or Morris method (Morris, 1991), since its computational demand is inexpensive, the parameter sensitivity is statistically quantified, and non-linear model responses can be determined (Morris, 1991; Campolongo et al., 2007). Moreover, parameters involved in parameter interactions and non-influential parameters can be identified.

Generally, the Morris method screens through a total sample size N where one parameter, or input factor $q = [q_i, ..., q_k]$, is changed while the others remain constant (one-at-a-time method). The total sample size N is generated based on r defined levels and q selected parameters such that $N = r(q + 1)$. Based on each sample, the elementary effects d_i is calculated with:

$$d_i(q) = \frac{f(q_i, ..., q_{i-1}, q_i + \Delta, q_{i+1}, ..., q_k) - f(q)}{\Delta} = \frac{f(q + \Delta e_i) - f(q)}{\Delta}, \tag{8}$$

where Δ represents the parameter step size, $q + \Delta e_i$ denotes the transformed parameter point, $q = [q_i, ..., q_k]$ is any selected parameter of N, and e_i consists of a vector of zeros but one in the i^{th} element. The local sensitivity of parameter q is described with the value of $d_i(q)$. For the global sensitivity, the statistical moments μ_i and σ_i as mean and standard deviation from the distribution of the total sample simulation are used (Morris, 1991). We use the absolute mean μ^* as proposed by Campolongo et al. (2007) to not disregard non-monotonic model responses because of opposite signs. The statistical moments for each set j are:

$$\mu_i^*(q) = \frac{1}{r} \sum_{i=1}^{r} |d_i^j(q)|, \tag{9}$$

$$\sigma_i(q) = \sqrt{\frac{1}{r-1} \sum_{i=1}^{r} (d_i^j(q) - \mu_i)^2}. \tag{10}$$

In this study, we quantify the model performance with the Kling-Gupta efficiency (KGE) (see Appendix A2 for the supplementary equations). Moreover, we apply the Latin hypercube sampling to guarantee a widespread input space. Using $r = 500$ and $q = 27$ parameters, the total sample size is $N = 14000$. We investigated all 27 parameters in Table 2 for the sensitivity analysis. To apply the elementary effects method, we implemented the equations of Morris (1991) and Campolongo et al. (2007) into a set of MATLAB scripts. The code is available on demand.

2.5 Coupled LAI-AET parameter optimization and benchmarking

The LAI-AET parameters are first optimized concerning different objectives, which are (i) a multi-objective optimization concerning LAI and AET ("upper benchmark"), (ii) an optimization only concerning observed LAI data ("LAI-obs"), and (iii) an optimization only concerning satellite-based GLASS-LAI data ("LAI-GLASS"). The model performance is then tested based on the benchmark proposed by Seibert et al. (2018), and the different objectives are compared. Seibert et al. (2018) have suggested using upper and lower model benchmarks to thoroughly evaluate the model performance of a specific modeling framework. In Seibert et al. (2018), the performance of the streamflow prediction is investigated. The application of a physical-based model is thereby compared to an upper (optimized, conceptual model) and lower benchmark (ensemble of random samples) (Seibert et al., 2018). To avoid an arbitrary good or bad model response from a single parameter set, like the default model parameters, Seibert et al. (2018) propose to use random parameter samples for the lower benchmark.

We apply the SCE-UA algorithm (Duan et al., 1994) to optimize the LAI-AET parameters. The SCE-UA is a genetic algorithm where samples of the parameters are stochastically generated first concerning the lower and upper bounds of the parameter values. The parameter values are then changed to develop the samples to an optimum, i.e., to the optimal value of an objective function. We use KGE to compare the simulated model output with the observed data. The algorithm application divides the initial sample into several sub-samples (complexes) (Duan et al., 1994). In each complex, varying combinations of parameter values are embedded. Each complex is then used to produce offspring using the downhill simplex procedure (Nelder and Mead, 1965). The probability of a parameter value being used in the following complex is proportional to its model fitness, i.e., to the objective function. The new offspring replace parameter values of lower fitness. The main advantage of the SCE-UA algorithm is the application of (i) mutation, where new parameter values in the defined parameter spaces can be spontaneously generated, and (ii) shuffling, where recombination of the parameter values in new complexes is conducted (Duan et al., 1994).

In this study, different objectives are defined for the LAI-AET parameter optimization (Table 4). First, the LAI-AET parameters are optimized in a multi-objective way with equal weight concerning observed AET and LAI ("upper benchmark"). This way, the performance potential of LAI-AET to fit both the AET and plant growth is quantified. Further, we also assess if a detailed plant growth optimization can predict AET using the single LAI optimization approaches ("LAI-obs" and "GLASS-LAI"). We use the SPOTPY toolbox (Houska et al., 2015) to apply the SCE-UA algorithm.

Table 4. Summary of benchmark elements, their optimization approach with the corresponding optimization objectives, and their evaluation. For the Lower benchmark, the median KGE of the AET performance of all 1000 random samples is used.

Benchmark element	Optimization approach	Objective(s)	Evaluation for benchmark
Upper benchmark	SCE-UA	Observed LAI & AET	AET
LAI-obs	SCE-UA	Observed LAI	AET
LAI-GLASS	SCE-UA	GLASS-LAI	AET
Lower benchmark	*Random sampling*	-	AET

All three optimization approaches are compared based on the individual AET evaluation using the benchmarking proposed by Seibert et al. (2018). The upper benchmark is defined to be the best potential model performance (here: "upper benchmark" in Table **??**). We generated 1000 uniformly distributed LAI-AET parameters samples for the lower benchmark, evaluated the simulated AET with observed AET, and determined the overall median KGE performance as the lower benchmark. With the upper and lower model limits, the AET prediction performance of optimizing the parameters only for LAI can be benchmarked for the footprint-scaled models of the forested and grassland region as well as for different PET methods (PET-HG, PET-PT, and PET-PM). With four benchmark elements (Table. 4), two land cover types, and three PET methods, 24 setups are compared to each other to assess the LAI-AET modeling performance of SWAT-T. In total, 27 parameters are considered for the sensitivity analysis. 22 of the initially defined 27 parameters are optimized to reduce the parameter space and address the equifinality problem. Five parameters are not changed but derived, e.g., from other regional studies. The groundwater parameters (GW_REVAP, RCHRG_DP, and REVAPMN) are obtained from Duku et al. (2015) who investigated the streamflow prediction with SWAT for the Bétérou catchment. The CN_2 numbers for FRSD and RNGE are derived from Alemayehu et al. (2017). The parameters HRU_SLP and SLSUBBN are catchment-specific and individually derived when a SWAT/SWAT-T model is setup. Hence, we kept these geospatial parameters constant for optimization.

3 Results

3.1 The relevance of a coupled LAI-AET parameter estimation

The influences of the parameter changes on both modeling objectives (LAI and AET) are displayed in Figure 3. The evaluation shows the distribution of the results from each parameter change for AET and LAI. All 27 parameters for all three used PET methods impact the simulated LAI and AET. Figure 3 shows examples of the parameters (EPCO, SOL_AWC, PHU, ALAI_MIN, DLAI, T_BASE) where the changes on both LAI and AET are the most significant using PET-PM in the forested region. The results for PET-HG and PET-PT are illustrated in the Appendix A1.

As shown in Figure 3, the variations for the parameter changes regarding intervals of the observed value are displayed. The AET and LAI data are clustered in 7 and 5 intervals, respectively. We used the same interval size for AET and LAI to improve readability. Each parameter change is then classified according to the interval. Then, the difference between observed and simulated data is calculated ($\Delta Y = Obs - Sim$). The distributions are computed based on the difference within the interval. If, for example, the observed values for the AET interval of 0.625 to 1.25 mm are compared with the simulated values of the EPCO changes, an overall AET difference of -2.2 to 1.2 mm can be observed. The parameters EPCO and SOL_AWC are commonly associated with AET modeling. Thus, large spreads in the AET model response for the parameter changes can be observed, e.g., the influence of EPCO is exceptionally high for values AET < 3 mm. Still, the influence of both parameters on the LAI simulation is indicated, too. For EPCO, decisive variations in the LAI response are observed for values LAI > 2 m^2/m^2. As the plant growth is close to the phase of maturity, the significance of the water uptake by the plant in SWAT-T (determined with EPCO) increases, and the importance of EPCO for LAI modeling can be observed. Generally, the EPCO parameter governs the actual transpiration, which, in turn, influences the water stress of plants and, thus, affects the actual plant growth. The impact

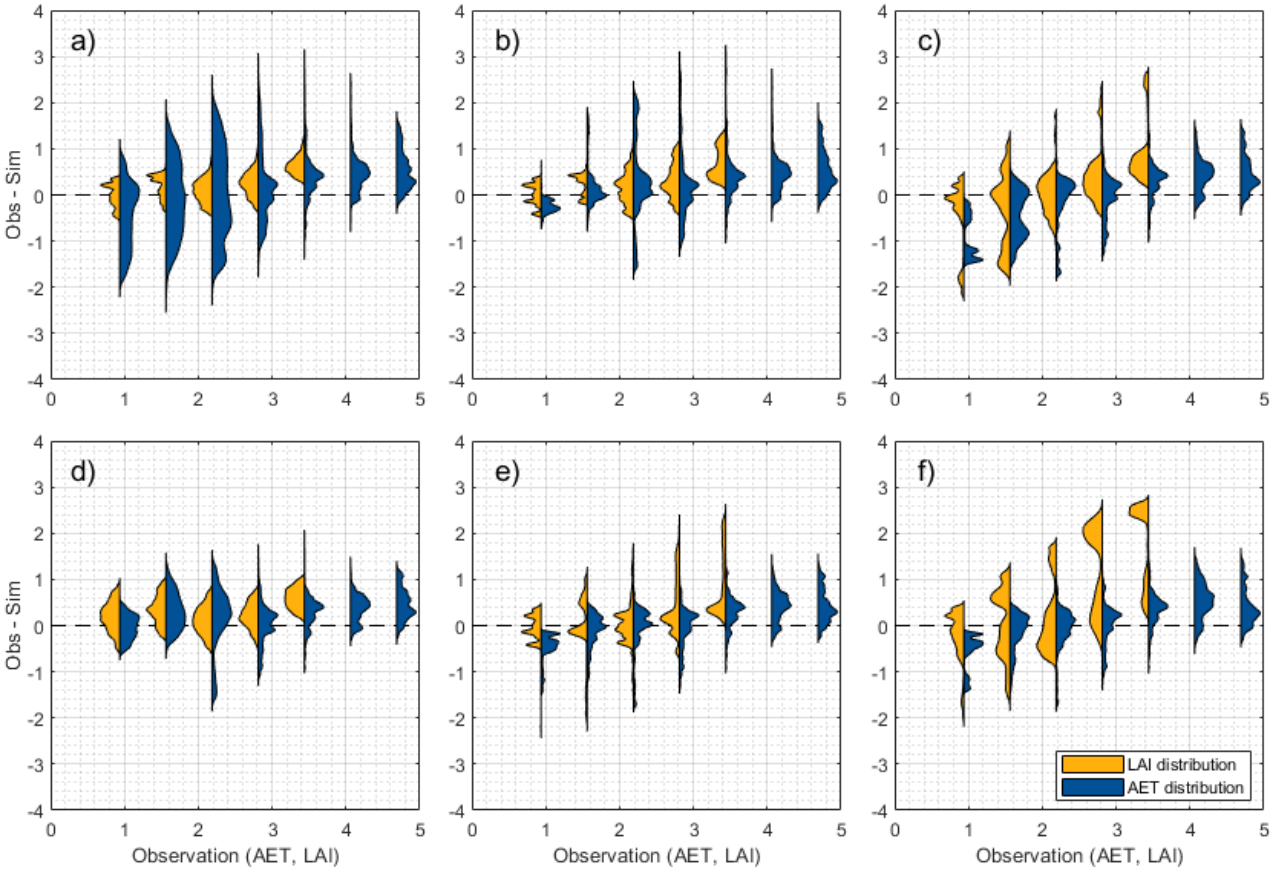

Figure 3. Distribution of variations in AET or LAI for the one-at-a-time parameter changes (1000 samples) for parameters a) EPCO, b) SOL_AWC, c) PHU, d) ALAI_MIN, e) DLAI, and f) T_BASE. The distributions are clustered in uniform intervals (size = 0.625) of the observed time series for AET [mm] or LAI [m^2/m^2]. The x-axis indicates the observed AET [mm] and LAI [m^2/m^2] values. The y-axis represents the difference between observed and simulated values with $\Delta Y = Obs - Sim$ regarding AET [mm] or LAI [m^2/m^2]. A perfect fit is indicated with the dashed line for $\Delta Y = 0$. Positive and negative values show an underestimation and overestimation of the simulated values, respectively. The distributions (violin plots) are created based on Karvelis (2024).

of EPCO on LAI is significant, especially during the wet season when essential AET rates occur. With high AET, the plant growth stress is intensified in this period. Similarly, the available water capacity in the soil layers (SOL_AWC) influences the LAI response more the further the plant is in the growing phase (LAI > 2 m^2/m^2). The EPCO and SOL_AWC parameters can limit and elevate plant growth in the wet season.

Concurrently, the shown LAI parameters (PHU, ALAI_MIN, DLAI, T_BASE) influence both AET and LAI. The variations of simulated AET regarding LAI parameter changes are particularly significant at the end of the wet and during the dry season (AET < 3 mm). PHU determines when the plant reaches maturity based on the heat unit assumption. Similarly, the DLAI parameter defines when the LAI begins to decline and, thus, the start of leaf senescence. If the maturity phase is too early

or short, the leaf senescence phase starts too early. In these cases for PHU and DLAI, the LAI-AET interaction is impaired, and influences on AET can be observed. The ALAI_MIN parameter defines the minimum LAI value for a plant type during the dormant period. If ALAI_MIN is set too small, the plant is underrepresented in the dry period, which results in low plant transpiration rates. The parameter changes for T_BASE result in the most extensive spread of simulated LAI values for all stages of the plant growth phase. With T_BASE, the temperature stress and the actual plant growth are determined in SWAT-T. The influence of the T_BASE parameter on AET is also present in the wet and dry periods of the AET modeling. Notably, the largest spreads of AET based on T_BASE can be observed for values AET < 3 mm.

The one-at-a-time parameter change evaluation and the LAI-AET cross-comparison show that AET parameters, such as EPCO or SOL_AWC, are significant for the AET and LAI modeling. Figure 3 also highlights that the LAI parameters, such as PHU, ALAI_MIN, DLAI, or T_BASE, can influence the AET model response. The variations in LAI and AET resulting from changes in the remaining 21 LAI-AET parameters (cf. Table 2) are similar, although not shown here. Hence, a coupled LAI-AET parameter estimation is essential for the reliable computation of LAI and AET, particularly for perennial land cover types in a sub-humid region in Western Africa.

3.2 LAI-AET parameter sensitivity analysis concerning observed LAI

The sensitivities of the LAI-AET parameters are quantified using the elementary effects method regarding the observed LAI data. Figure 4 shows the statistical moments μ^* and σ for each parameter. It can be observed that nearly all parameters are located close or slightly above the 1:1 line, which defines a non-linearity of the parameters (Garcia Sanchez et al., 2014). Albeit some exceptions, the parameters in the forested region result in higher σ values, implying that the parameter interactions are more non-linear than in the grassland region. Generally, proximity of the parameter sensitivities for each land cover type method can be observed, e.g., the diamond symbols for forest are close. Thus, differences between the PET methods and for the same land cover type are insignificant, suggesting potential independence of the LAI parameter sensitivity from the PET method. Moreover, all three groundwater parameters result in values $\mu^* = 0$, thus insensitive to plant growth. Hence, they are excluded from the in-depth parameter analysis below.

Moreover, all PET methods are clustered to compare the sensitivity of the LAI-AET parameters for different land cover types. Figure 5 shows the distribution of μ^* where all PET methods are combined in one land cover group. The parameters are ranked according to the mean μ^* values from the simulations in the forested region. In Figure 5, it can be observed that the general parameter sensitivity patterns are similar in the forested and grassland region, albeit with differences in the magnitude of μ^* for the land covers. The most sensitive parameters for both land use types are T_BASE, PHU, DLAI, BLAI, and SOL_RD. Moreover, a high boxchart (high spread of μ^* values) implies a high parameter interaction. The boxplot heights for the forest and grassland clusters are generally comparable for the same parameters. If a parameter (e.g., T_BASE) in the forest region shows meaningful interactions, responses are also indicated for the same parameter in the grassland region alike. However, the parameters BLAI and SOL_RD appear to have higher parameter interactions in the forest than in the grassland region. Although the ranking is shown in Figure 5 concerning the mean μ^* values resulting from the forested region, the sensitivity hierarchy of the forested and grassland clusters are generally interchangeable.

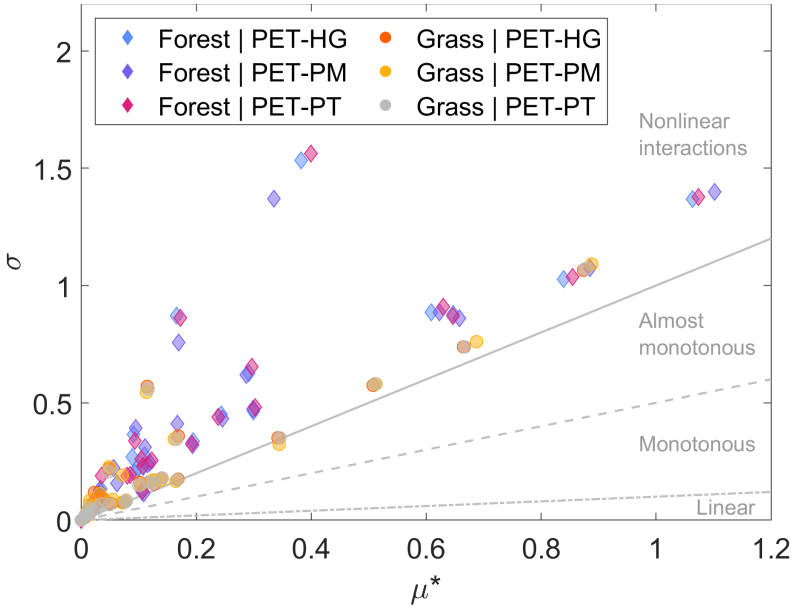

Figure 4. The statistical moments μ^* and σ of the elementary effects for the evaluation of the LAI-AET parameter sensitivity concerning observed LAI. We use the relation of σ/μ^* to classify regions of non-linear, almost monotonous, monotonous, and linear parameter behavior (Garcia Sanchez et al., 2014).

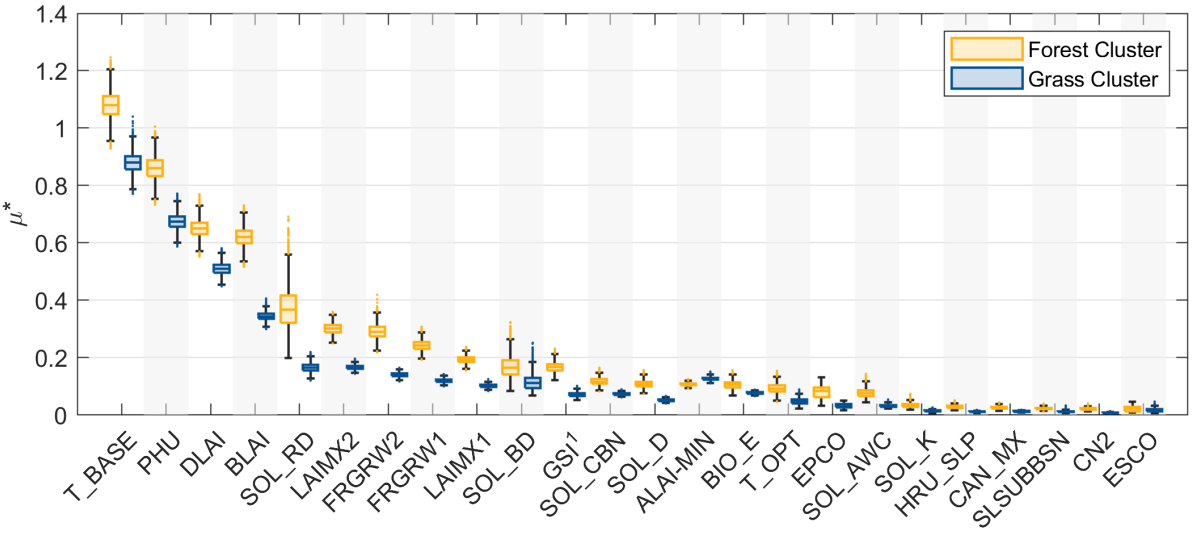

Figure 5. Clustering of the sensitivity analysis of all PET methods in the land cover types forest and grassland concerning observed LAI. The parameters are sorted according to the mean μ^* values resulting from the forested region. [1]Parameter GSI is only accounted for when PET-PM is used.

From Figure 5, a clear ranking pattern for PET methods and land use types can be observed (see also Figure A4). Variations in the ranking position for each parameter are thereby minor, albeit some exceptions for ALAI_MIN, GSI, EPCO, and ESCO. Prior in Figure 3, the influence of EPCO on LAI has been qualitatively illustrated. Here, the parameter sensitivity of EPCO on LAI is quantified with μ^* and ranked with the other parameters in Figure 5. The ranking differs for EPCO, GSI, and ESCO when PET-PM is used (Figure A4). Its application implies that EPCO and ESCO are less while GSI is more relevant to the LAI model output. The stomatal conductance GSI is only accounted for in SWAT-T when PET-PM is used. Concurrently, the ALAI_MIN parameter is higher ranked for grassland than for forest. Lower LAI values in the dry period of the rainy season increase the parameter ranking of ALAI_MIN. Ultimately, the plant growth parameters are generally higher ranked than the AET parameters. Still, the ranking of SOL_RD, SOL_BD, SOL_CBN, SOL_D, and EPCO indicate an observable influence of AET parameters also on LAI. The sensitivity analysis of the LAI-AET parameters highlights that a coupled LAI-AET parameter estimation is inevitable for a comprehensive assessment of perennial plant growth of SWAT-T in sub-humid regions for all 3 PET methods.

3.3 Optimization and benchmark test of the LAI-AET modeling

The SCE-UA algorithm is applied to optimize the LAI-AET parameter in a multi-objective way (upper benchmark) and only concerning observed (LAI-obs) as well as satellite-based (LAI-GLASS) LAI data. The evaluation focuses on observed AET in the following. The upper benchmark optimization results in very good modeling results for the three PET methods and two land cover types. For all six setups, the model performance (AET) of the upper benchmark is $KGE \geq 0.75$ (Table 5). The performance of the LAI optimization to simulate AET results in values of $KGE \geq 0.44$ (LAI-obs) and $KGE \geq 0.49$ (LAI-GLASS).

Table 5. Summary of final KGE values concerning observed AET and LAI for the benchmark elements. For the lower benchmark, the median AET performance of all 1000 random samples is determined. For LAI modeling, the LAI-GLASS optimization is investigated with the GLASS-LAI. The lower benchmark LAI values are based on the parametrization of the median AET performance runs.

PET method	Upper benchmark		LAI-Obs		LAI-GLASS		Lower benchmark	
	Forest	Grassland	Forest	Grassland	Forest	Grassland	Forest	Grassland
Final KGE values regarding AET performance								
PET-HG	0.75	0.87	0.44	0.69	0.57	0.71	0.45	0.73
PET-PM	0.84	0.93	0.77	0.71	0.49	0.87	0.46	0.72
PET-PT	0.76	0.90	0.68	0.82	0.60	0.71	0.47	0.74
Final KGE values regarding LAI performance								
PET-HG	0.84	0.87	0.94	0.91	0.96	0.88	-0.47	0.17
PET-PM	0.93	0.89	0.94	0.90	0.94	0.94	-0.04	0.07
PET-PT	0.93	0.89	0.95	0.90	0.96	0.90	-0.39	0.02

The median of the random sampling (lower benchmark) determines values of $KGE = 0.45$ to 0.74 across all six setups for AET. In the forested region, LAI-obs and LAI-GLASS yield better predictions of AET than the lower benchmark, except for the PET-HG application and LAI-obs optimization. Still, this difference is negligible. Hence, a single optimization with LAI (observed or GLASS-LAI) can improve the AET estimation in forested regions. The lower benchmark outperforms the LAI optimization (observed and GLASS-LAI) in the grassland setups, although only in minor KGE differences. Considering that $KGE \geq 0.5$ is often accepted as a behavioral model performance (Rogelis et al., 2016; Knoben et al., 2019), the resulting KGE values for AET in the grassland setups are still satisfying. Figure 6 shows the corresponding time series for AET. An overestimation of AET (PET-HG method), particularly in the wet period in the grassland region for the LAI optimization, can be observed. An underestimation of AET in the wet period is computed for the PET-PM method.

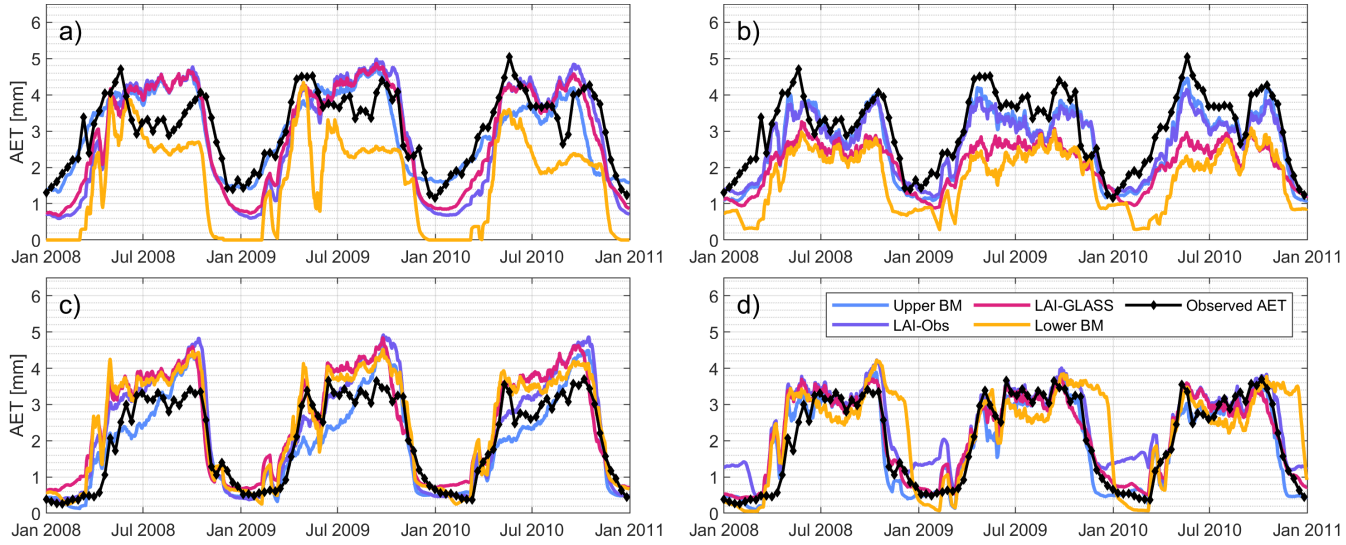

Figure 6. Time series of simulated and observed AET for the four benchmark elements, with: a) PET-HG method in the forested region, b) PET-PM method in the forested region, c) PET-HG method in the grassland region, and d) PET-PM method in the grassland region.

Generally, the best model performance is achieved by applying PET-PM independent of the land cover type. The good AET fit for the LAI optimization approaches is explained by LAI being a term used in calculating the canopy resistance in the PET-PM equation and the dynamic plant growth cycle. The LAI optimization guarantees a steady transpiration rate even in the dry period without the plant dying, i.e., LAI dropping to zero. The lower benchmark with no tailor-suited LAI modeling outputs an underestimation of AET in the dry season (Figure 6), which can be attributed to its low LAI values in this season (Figure 7). The simulated LAI and AET data for PET-PT are similar to the PET-HG results (cf. A5). Concurrently, good model performance for PET-PM is achieved for the lower benchmark, too. Although an insufficient LAI modeling results for the lower benchmarks in the grassland region, acceptable AET performance is still achieved (Table 5). Ultimately, the results show that SWAT-T can make accurate LAI and AET predictions. Moreover, the benchmark test shows that even if no AET data is available, the LAI parameter optimization with observed or satellite-based LAI facilitates an acceptable AET estimation in

forest and grassland regions. However, the AET performance from LAI calibration is constrained by the hydro-meteorological data availability for the choice of the PET method and if the application of energy-based PET methods, particularly PET-PM, is feasible.

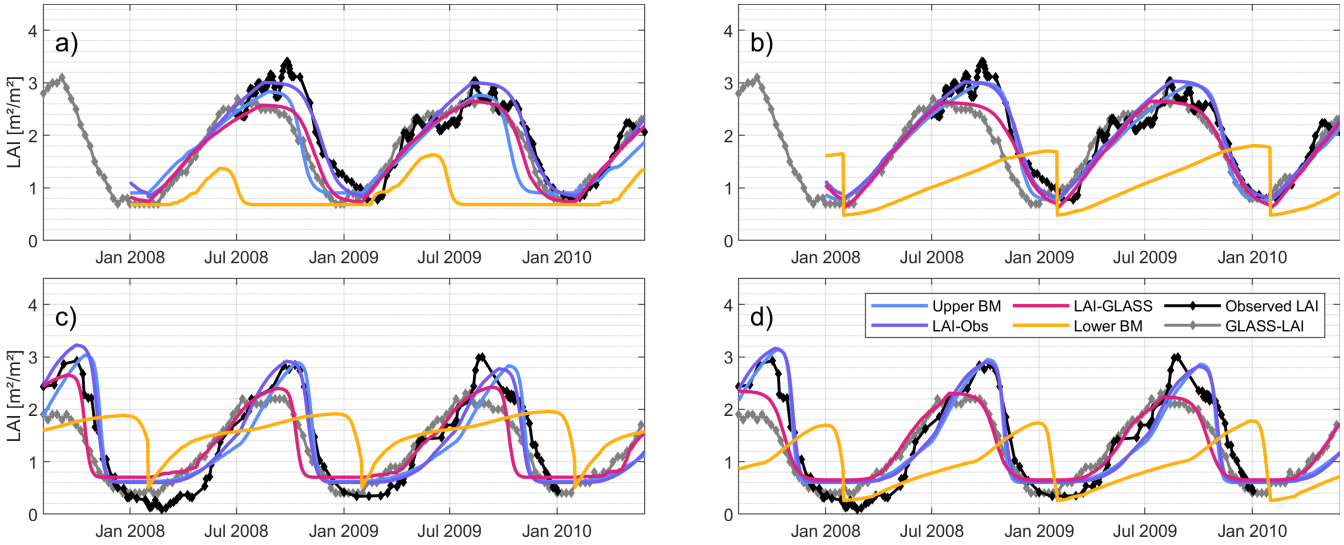

Figure 7. Time series of simulated, observed and remotely sensed AET for the four benchmark elements, with: a) PET-HG method in the forested region, b) PET-PM method in the forested region, c) PET-HG method in the grassland region, and d) PET-PM method in the grassland region.

4 Discussion and outlook

4.1 Evaluation of the LAI-AET parameters with observed and GLASS-LAI

This study evaluates the LAI modeling with observed and satellite-based LAI data. Previous studies with SWAT have also employed field measurements for LAI (Park et al., 2017; Yang et al., 2018; Nantasaksiri et al., 2021) or forest biomass production (Khanal and Parajuli, 2014; Haas et al., 2022) to evaluate the LAI modeling of SWAT. However, the parameters differ in these studies, e.g., the total number of parameters applied ranges from three (Yang et al., 2018) to 18 (Haas et al., 2022). The suggested LAI parameter list for SWAT-T in Alemayehu et al. (2017) consists of 11 parameters. We applied one-at-a-time parameter changes to assess the interaction of LAI and AET parameters on both simulated LAI and AET data. We compared the resulting model responses (LAI, AET) for each parameter change and figured the influences of LAI parameters on AET modeling and vice versa. Although the assessment of the one-at-a-time changes was based on a qualitative analysis, a clear pattern of the reciprocal influences became apparent. Hence, we extended the LAI parameter list and identified 27 LAI-AET parameters for evaluation of the significance of LAI on the AET estimation in SWAT-T.

We applied the elementary effects method to evaluate the parameter sensitivity to understand the parameter interactions in SWAT-T with observed LAI data. Previous efforts to assess the sensitivity of LAI parameters have focused on a relative sensitivity index (Khanal and Parajuli, 2014; Nantasaksiri et al., 2021). In the present study, the sensitivity of the comprehensive set of 27 LAI-AET parameters is quantified with the elementary effects method in SWAT-T for the first time. Before, the Morris screening was used for the sensitivity analysis of SWAT model parameters only concerning discharge (Xiang et al., 2022; Abbas et al., 2024). With the application of the Morris screening, a ranking of the sensitivity of the parameters is determined in the present study. The most influential parameters on LAI are T_BASE, PHU, DLAI, and BLAI, independent of the land cover type or the PET method. Moreover, SOL_RD is the parameter with the highest influence on the other parameters. Its influence is significant because it defines the root depth within the soils, which in turn determines the plant water uptake and, thus, the growing efficiency. The impact of SOL_RD is significant in the forested region where the uptake of plants is high, and the roots are growing deep. The sensitivities reported in Khanal and Parajuli (2014) are highest for the parameters DLAI, BIO_E, BLAI, and SOL_RD. Nantasaksiri et al. (2021) identified the parameters BIO_E, HVSTI, BLAI, $LAIMX_2$, and DLAI to be the most sensitive. The findings in both studies are coherent with our results, albeit the missing investigation of some of the most sensitive parameters, e.g., T_BASE and PHU. Moreover, we apply a global sensitivity measure while Khanal and Parajuli (2014) and Nantasaksiri et al. (2021) have used a local measure (relative sensitivity index). However, local measures are limited if the model response is nonlinear (Saltelli et al., 2008), which is the case for the LAI-AET parameters concerning observed LAI (Figure 4). Thus, we could detect and address the non-linearity of the LAI-AET parameters with the elementary effects method in the present study.

The field measurements used in this study are derived from hemispherical photographs and satellite-based corrections. Such assorted LAI data can be subject to uncertainties (Fang et al., 2019). To address the potential shortcomings of LAI observations, we additionally evaluated the LAI estimation regarding satellite-based GLASS-LAI. For both land cover types, the performance of the LAI prediction is thereby accurate independent of the PET method. We applied the GLASS-LAI data since it is reliable in different regions worldwide (Liang et al., 2014) and robust to noise and uncertainties satellite-based vegetation can be susceptible to in tropical regions (Viovy et al., 1992; Atkinson et al., 2012). The dual consideration of both observed and GLASS-LAI data ensured the comprehensive LAI evaluation in the present study.

4.2 Optimization and benchmarking of the AET modeling with observed AET on the footprint scale

The model extent of the grassland region (2300 m^2) represents the actual footprint size of 4000 m^2 estimated by Mamadou et al. (2014) well. The footprint for the forested region is seasonally varying and can be up to 60000 m^2 (Mamadou et al., 2014). Generally, the source area of AET in EC systems can fluctuate over the year (Kim et al., 2018) because of, for example, the wind direction where the windrose can influence the extent of the footprint (Chen et al., 2009; Chu et al., 2021). Since the model extents of SWAT-T are constant for the modeling period and the necessary data was unavailable, we approximated the model scale to represent the footprint for the whole season according to Chu et al. (2021). The main objective of the present study is the thorough evaluation of the vertical fluxes (AET) based on the LAI-AET interaction in SWAT-T. In SWAT/SWAT-T, the vertical fluxes (AET) are computed on the HRU level. Hector et al. (2018) investigated the same regions using a physically

based model for the critical zone (ParFlow-CLM) and also concluded the significance of vegetation on the AET estimation, which is coherent with our findings.

In the present study, we also investigated whether a detailed LAI modeling disregarding AET can predict reliable AET estimates in SWAT-T. We showed that the LAI optimization also facilitates an adequate behavioral modeling of AET with acceptable KGE values for both land cover types. However, evaluating the model performance where only the values of one efficiency metric (e.g., KGE) are considered can be misleading because the explanatory power of the model is missing (Schaefli and Gupta, 2007; Knoben et al., 2019). The information if a modeling approach is applicable or should be rejected and the assessment of the strengths and deficiencies of the modeling approach needs to be covered in pure values of one efficiency metric (e.g., KGE) (Knoben et al., 2019). To address these shortcomings of an exclusive KGE value evaluation, we applied the benchmark test proposed by Seibert et al. (2018). The comparison of modeling approaches, such as the single LAI optimization with upper and lower benchmark levels, facilitated the assessment of whether a detailed LAI modeling (single LAI optimization) can improve the LAI prediction in SWAT-T. The benchmarking showed that the significance of a thorough LAI modeling is more pronounced in the forested than in the grassland region.

4.3 Impacts of the model structure on the AET estimation

On the daily time-step, the temporal dynamics of simulated AET fit adequately to the observed AET pattern in the dry and wet season for all three PET methods. Thereby, the application of PET-PM outperforms PET-HG and PET-PT. Generally, the PET-PM application is more physically complex than PET-HG and PET-PT but requires more input data. The computation of PET-HG and PET-PT relies on empirically delineated coefficients, e.g., H_0 and α_{pet}, respectively. In PET-PM, terms for different properties of the land-atmosphere interaction are implemented, such as vapor pressure or the canopy r_c and aerodynamic resistance r_a. In PET-PT however, the aerodynamic term α_{pet} is modeled with a constant coefficient of 1.28 (Neitsch et al., 2011). Moreover, the partitioning of PET into potential plant transpiration and soil evaporation is threshold based in PET-HG and PET-PT. While PET-PM estimates the potential transpiration using the PM equation where r_c and r_a are dependent on the LAI modeling, the partitioning of PET implemented in PET-PT and PET-HG is based on the threshold $LAI > 3.0$. Hence, the significance of detailed LAI modeling in these methods has less impact on plant transpiration. For the forested region, the LAI modeling (single LAI optimization disregarding AET) can still predict the AET adequately. The influence of LAI estimation is less substantial in the grassland region, where the lower benchmark (random sampling) outperforms the single LAI optimization (observed and GLASS-LAI). However, the physical representation of the LAI-AET relationship is limited since low KGE values are computed. Overall, the more straightforward approaches PET-HG and PET-PT can still yield adequate AET outputs (Archibald and Walter, 2014), although PET-PM offers a more physically sound depiction of the LAI-AET interaction.

In previous studies, similarly accurate AET performances for the PET-PM application were observed for a forested region (Ferreira et al., 2021) and for a grassland region (Qiao et al., 2022) regarding a comparison with AET from EC systems. An improvement of the AET estimation with SWAT-T using EC systems has also been demonstrated for PET-HG, PET-PT, and PET-PM on the HRU scale in López-Ramírez et al. (2021) where the annual budgets for AET fit best for PET-HG (López-

Ramírez et al., 2021). However, no coupled LAI-AET parametrization has been considered. We were able to address the relevance of the coupled LAI-AET parametrization and thereby also demonstrated the best overall performance for PET-PM.

4.4 Outlook

The elementary effects were computed based on the period for which measured LAI data is available. SWAT-T divides plant growth into four phases (start of growing, maturity, leaf senescence, dormancy). A time-varying sensitivity analysis of the LAI-AET parameters concerning the plant growth phases should be done in future work. Applications should explore approaches such as dynamic identifiability analysis (Wagener et al., 2003) or wavelet-based methods (Chiogna et al., 2024). These time-varying approaches can further improve understanding the LAI-AET parameter interaction.

We showed that the LAI-AET modeling of SWAT-T for approximated footprints is applicable for perennially vegetated regions in Western Africa. In future work, the coupled LAI-AET modeling should be transferred from the footprint to the catchment scale. The water balance of the ecosystems of Western Africa is mainly characterized by a high share of AET. Hence, this study focuses on analyzing the LAI-AET interaction and, thus, on the dominant vertical fluxes in these regions. Given the significance of AET in Western Africa, the LAI-AET relationship can also be essential to estimate the horizontal fluxes that are substantial for the streamflow computation on the catchment scale. Applying satellite-based LAI data, e.g., GLASS-LAI, can also support plant growth and AET modeling on larger scales. Moreover, we focused our analysis on characteristic regions of Western Africa. Future work should analyze the LAI-AET interaction for other land cover types, e.g., regions with higher LAI values like the Congo forests or other climatic zones, such as energy-limited regions.

The present study focuses on LAI as a vegetation attribute. In SWAT/SWAT-T, the canopy height is modeled, too. The canopy height can impact the PET estimation, e.g., in the application of PET-PM, where the canopy resistance r_c is a function of the canopy height. Moreover, EC systems can also offer other relevant attributes of the vegetation-AET interaction, such as derivations of the aerodynamic conductance, surface conductance, water vapor, heat fluxes, or the evaporative fraction (Mamadou et al., 2016). These attributes improve the physical understanding of the vegetation-AET interaction and can also be valuable to inform hydrological modeling (Hector et al., 2018). We focused on the application of LAI because (i) it is a key vegetation attribute in SWAT-T, and (ii) global products of LAI are available. Since the seasonal dynamics of both forest and grassland vegetation (LAI) are modeled accurately, we postulate that the approaches of this study can be transferred to other plant and crop types.

Considering a coupled LAI-AET parametrization, the quantification of biomass or crop yield for other plant species can be addressed, too. Yang and Zhang (2016) investigated the biomass/primary productivity with SWAT for different flux sites of the AmeriFLUX network. They identified BIO_E, BLAI, T_OPT, T_BASE, and BIO_LEAF as the most significant parameters for biomass. Apart from the BIO_LEAF, the choice of parameters is similar to our study. Hence, LAI modeling can also be used as a proxy for biomass estimation. Still, in-depth analysis with observed biomass data is inevitable if the modeling objective is the evaluation of biomass and net primary productivity.

5 Conclusion

The broad implication of this research is the presentation of a comprehensive LAI-AET parameter evaluation to model both LAI and AET using an eco-hydrological model. We highlighted the relevance of a coupled LAI-AET parameter estimation in SWAT-T. Although the impact of LAI parameters on the AET prediction can be low, substantial influence can be observed on the AET dynamics. The impact of the LAI parameters on AET is exceptionally high at the end of the wet season and the beginning of the dry season, when the plant growth phase shifts from plant maturity to leaf senescence. Moreover, water stress on plant growth resulting from the AET estimation can be decisive and should be considered for comprehensive LAI modeling. We conclude that the relevance of a coupled LAI-AET parameter estimation indicates that a stepwise modeling approach (e.g., first LAI, afterward AET) requires a careful review of the simulated LAI after the AET parameters are estimated. The analysis of the elementary effects method demonstrates that most LAI parameters behave non-linearly if compared to observed LAI data. The most sensitive parameters for LAI modeling are those associated as LAI parameters. However, the Morris screening also indicates a meaningful contribution of the soil parameters. The ranking further illustrates the independence of the LAI parameters to the land cover type (forest and grassland).

The multi-objective optimization with the SCE-UA algorithm results in accurate estimations of both LAI and AET for all PET-methods and land cover types. SWAT-T has also been proven applicable on the footprint scale in Western Africa. Although the simpler PET-HG and PET-PT methods facilitate satisfactory modeling results, applying the PET-PM method outperforms these methods for the LAI and AET estimation in the forested and grassland regions. Moreover, our work demonstrates that an adequate estimation of AET can be obtained if the LAI-AET parameters are only optimized concerning LAI data (and disregarding AET data) for forest and grassland regions. Compared to the lower benchmark level, the benchmark test illustrates an enhancement of the AET prediction for the PET-methods (particularly PET-PT and PET-PM). This is particularly noteworthy for data-scarce regions where no field measurements of AET are available. Even if no observed LAI data for a forested region is available, practitioners and researchers can optimize the LAI-AET parameters using remotely sensed LAI data and still achieve reliable AET estimations. In the grassland region, the resulting AET prediction from the LAI optimization is adequate, too. However, the lower benchmark indicates a better performance for the grassland site. The good result of the lower benchmark is obtained from the median KGE performance of a large number of parameter samples (1000 runs). Single parameter changes, mean, or the default model parameter values of the SWAT/SWAT-T crop database do not necessarily facilitate a satisfactory AET prediction. Overall, the LAI-AET parameter optimization for grassland yields a sufficient AET performance. Nevertheless, its role in the AET estimation is less critical than for forested regions.

Finally, we stress the importance of opting for a coupled parameter estimation to understand the LAI-AET interaction and to improve the land-atmosphere simulation in hydrological modeling. The performance comparison of modeled AET confirms that a detailed plant growth analysis is essential. The highlighted relevance of the LAI-AET interaction is significant for a thorough quantification of hydrological processes and, hence, necessary for the comprehensive assessment of water resources management.

Appendix A: Appendix

A1 Appendix A1 - Figures

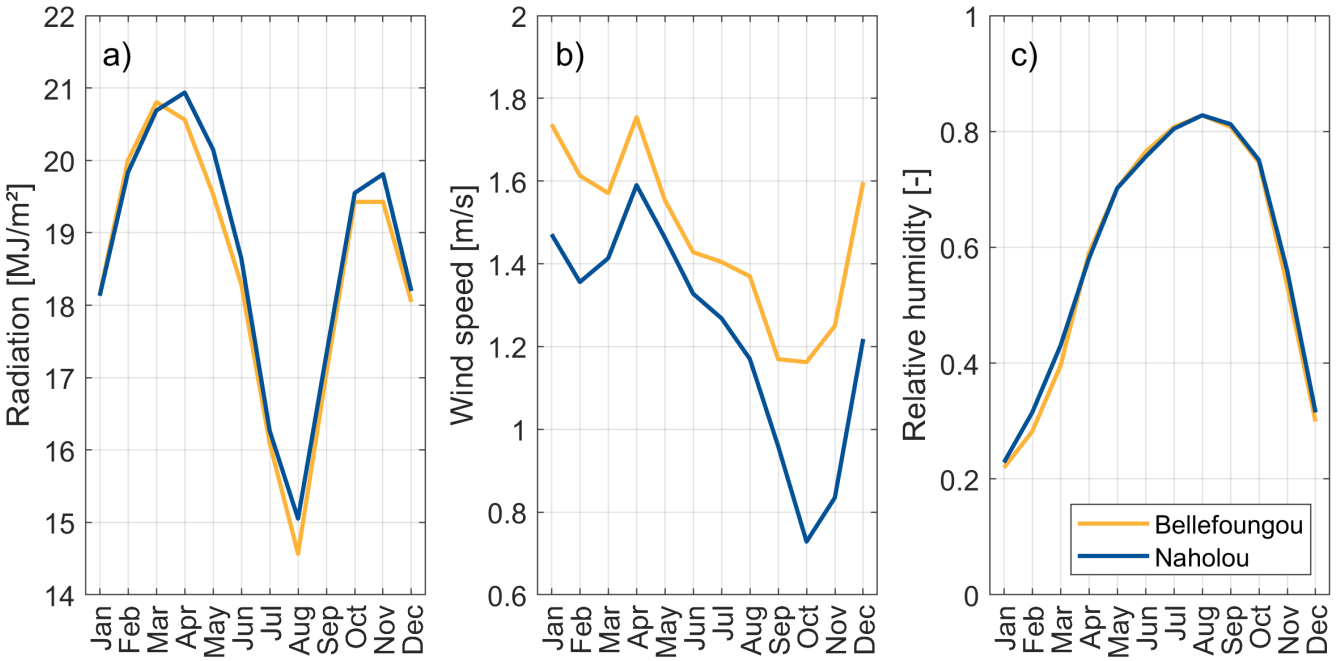

Figure A1. Seasonality of a) daily total solar radiation, b) wind speed, and c) relative humidity for the study sites Bellefoungou (forest) and Naholou (grass). The seasonality is derived from measurements of each eddy covariance system.

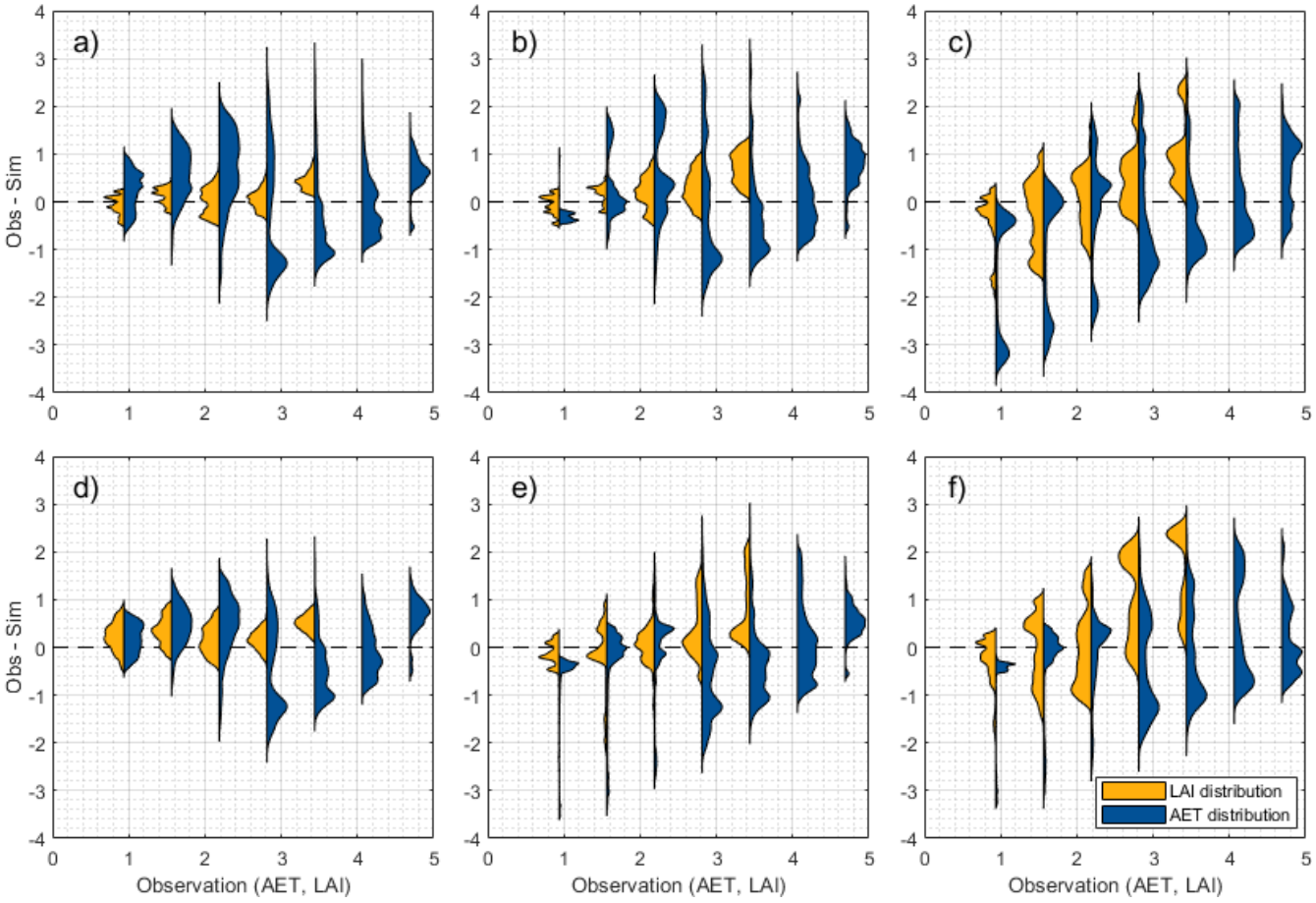

Figure A2. Distribution of variations in AET or LAI for the one-at-a-time parameter changes for PET-HG for parameters a) EPCO, b) SOL_AWC, c) PHU, d) ALAI_MIN, e) DLAI, and f) T_BASE. The distributions are clustered in uniform intervals (size = 0.625) of the observed time series for AET [mm] or LAI [m^2/m^2]. The x-axis indicates the observed AET [mm] and LAI [m^2/m^2] values. The y-axis represents the difference between observed and simulated values with $\Delta Y = Obs - Sim$ regarding AET [mm] or LAI [m^2/m^2]. A perfect fit is indicated with the dashed line for $\Delta Y = 0$. Positive and negative values show an underestimation and overestimation of the simulated values, respectively. The distributions (violin plots) are created based on Karvelis (2024).

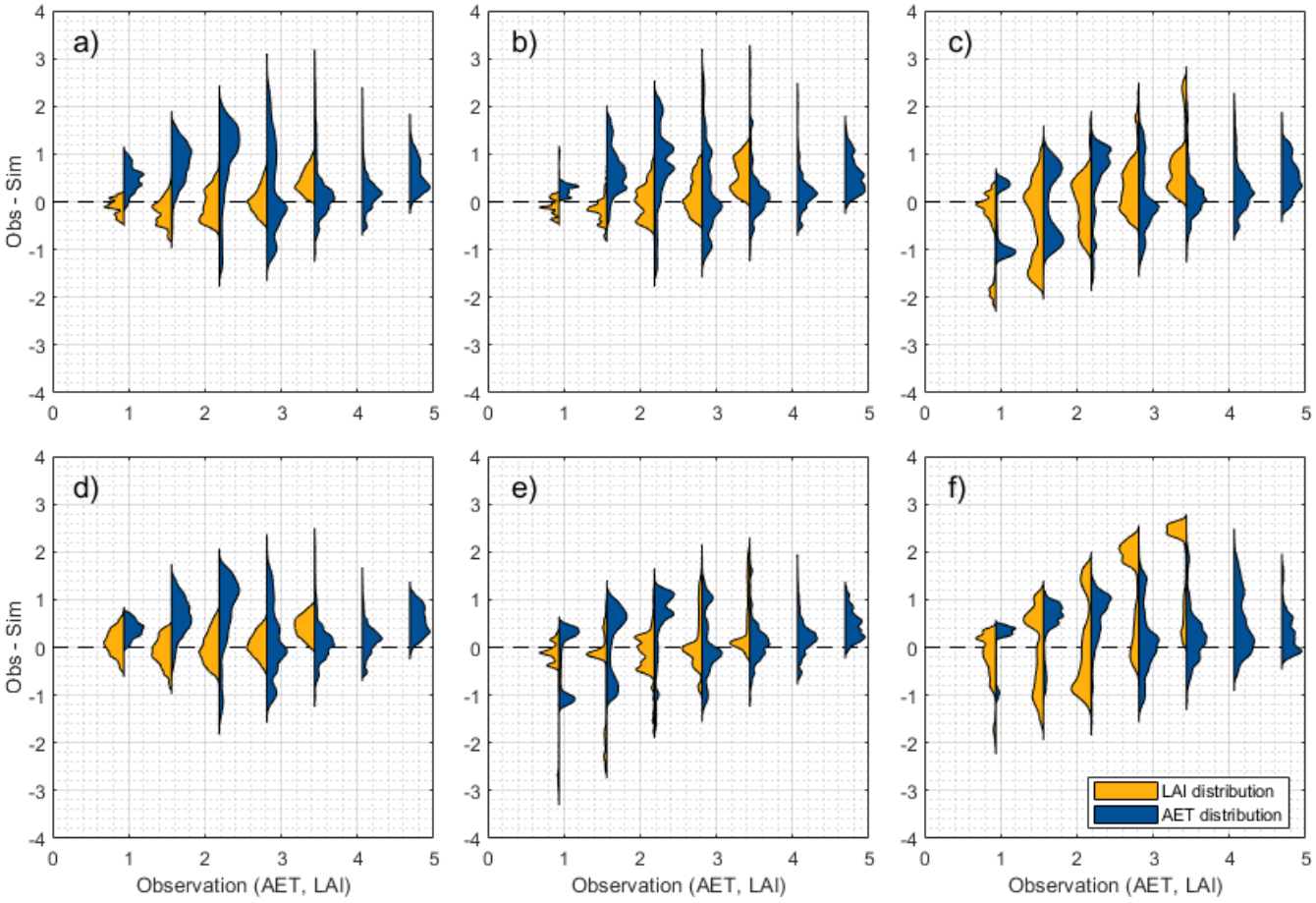

Figure A3. Distribution of variations in AET or LAI for the one-at-a-time parameter changes for PET-PT for parameters a) EPCO, b) SOL_AWC, c) PHU, d) ALAI_MIN, e) DLAI, and f) T_BASE. The distributions are clustered in uniform intervals (size = 0.625) of the observed time series for AET [mm] or LAI [m^2/m^2]. The x-axis indicates the observed AET [mm] and LAI [m^2/m^2] values. The y-axis represents the difference between observed and simulated values with $\Delta Y = Obs - Sim$ regarding AET [mm] or LAI [m^2/m^2]. A perfect fit is indicated with the dashed line for $\Delta Y = 0$. Positive and negative values show an underestimation and overestimation of the simulated values, respectively. The distributions (violin plots) are created based on Karvelis (2024).

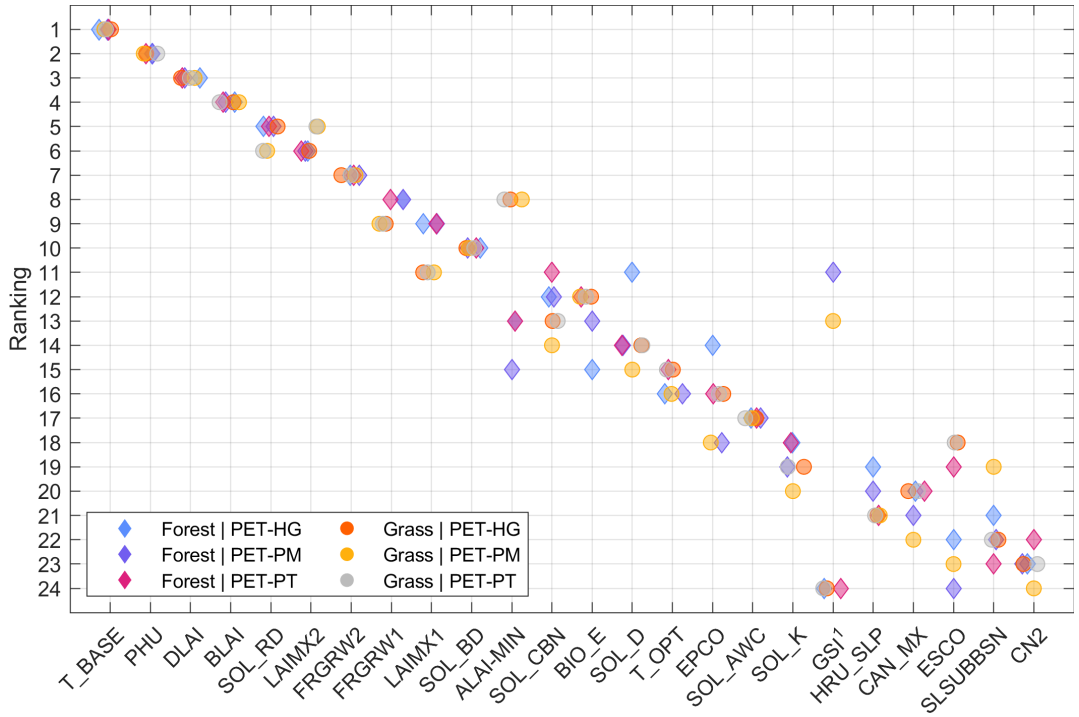

Figure A4. Ranking of the LAI-AET parameter sensitivity for the three PET methods and two land cover types concerning observed LAI. [1]Parameter GSI is only accounted for when PET-PM is used.

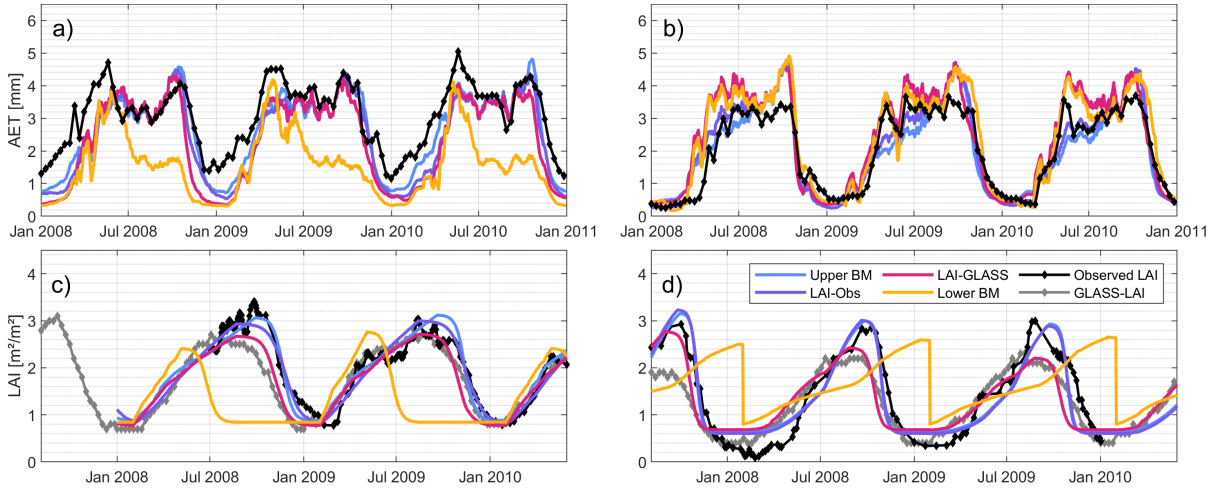

Figure A5. Time series of simulated and observed AET and LAI for the four benchmark elements computed with the PET-PT method, with: a) AET in the forested region, b) AET in the grassland region, c) LAI in the forested region, and d) LAI in the grassland region.

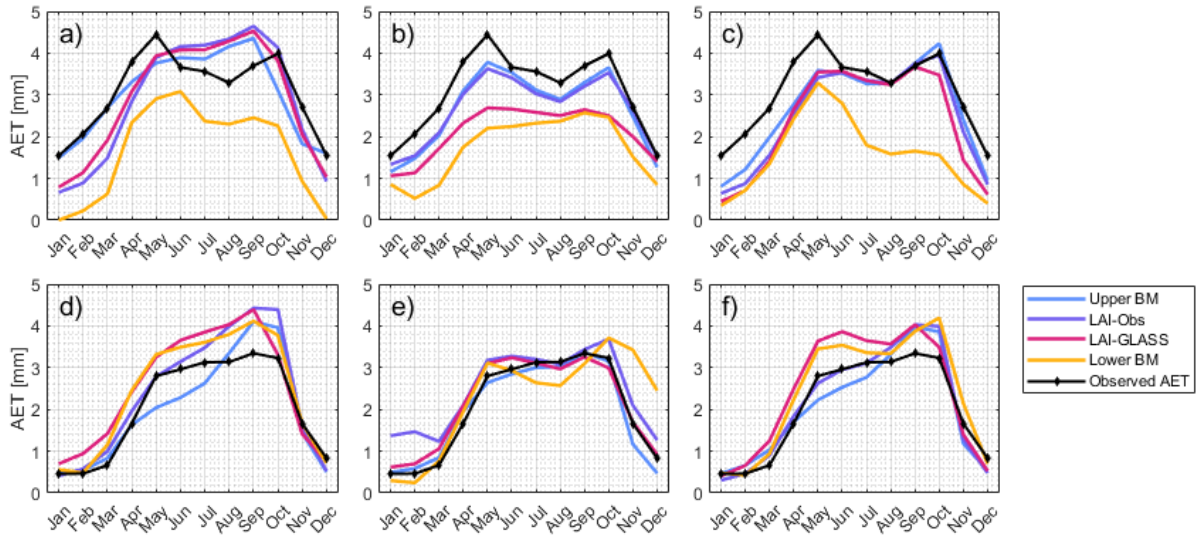

Figure A6. Seasonality of the simulated and observed AET time series. The top row (a-c) shows the AET data for the forested region for different PET-methods, with applications of a) PET-HG, b) PET-PM, and c) PET-PT. The bottom row (d-f) shows the grassland region, with applications of d) PET-HG, e) PET-PM, and f) PET-PT.

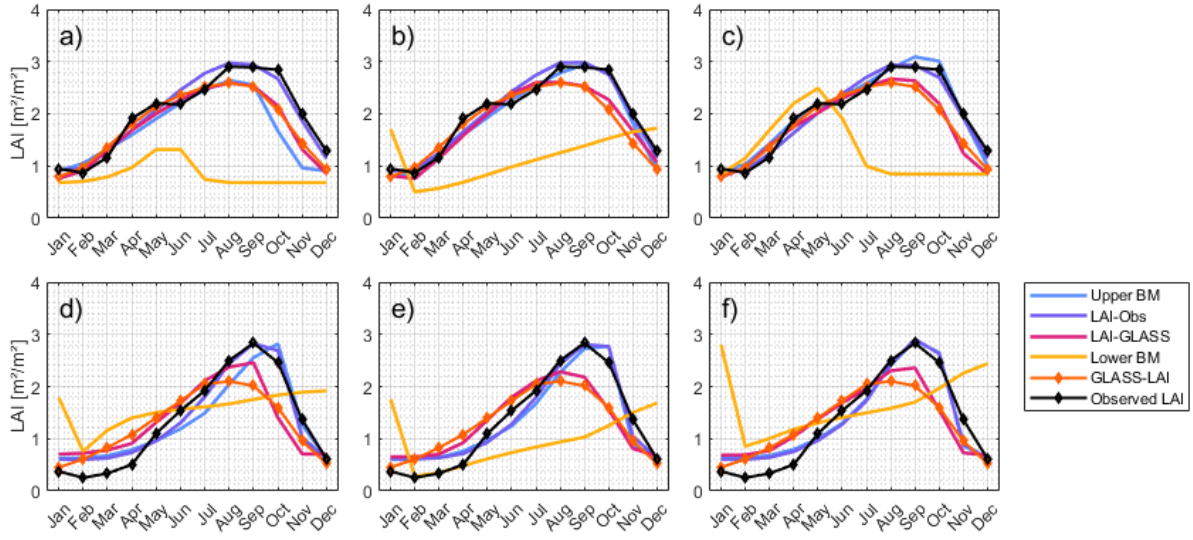

Figure A7. Seasonality of the simulated and observed LAI time series. The seasonality for LAI-obs as well as GLASS-LAI are displayed. The top row (a-c) shows the LAI data for the forested region for different PET-methods, with applications of a) PET-HG, b) PET-PM, and c) PET-PT. The bottom row (d-f) shows the grassland region, with applications of d) PET-HG, e) PET-PM, and f) PET-PT.

A2 Appendix A2 - Supplementary equations

Water stress $wstrs$ is calculated as:

$$wstrs = 1 - \frac{E_{t,act}}{E_t} = 1 - \frac{w_{actualup}}{E_t}, \tag{A1}$$

where $E_{t,act}$ is the actual transpiration, E_t is the potential plant transpiration, and $w_{actualup}$ is the total water uptake. $w_{actualup}$ is computed based on the amount of water in the soil layer and the water content at the wilting point (for details refer to Neitsch et al. (2011)).

Temperature stress $tstrs$ is calculated as:

$$tstrs = \begin{cases} 1, & \text{if } T_{av} \leq T_{base} \\ 1 - exp\left(\frac{-0.1054 \cdot (T_{opt} - T_{av})^2}{(T_{av} - T_{base})^2}\right), & \text{if } T_{base} < T_{av} \leq T_{opt} \\ 1 - exp\left(\frac{-0.1054 \cdot (T_{opt} - T_{av})^2}{(2 \cdot T_{opt} - T_{av} - T_{base})^2}\right), & \text{if } T_{opt} < T_{av} \leq 2 \cdot T_{opt} - T_{base} \\ 1, & \text{if } T_{av} > 2 \cdot T_{opt} - T_{base} \end{cases} \tag{A2}$$

where T_{av} is the mean air temperature for the day, T_{base} is the base temperature of the plant for growth, and T_{opt} is the optimal temperature of the plant for growth.

Nitrogen stress $nstrs$ is calculated as:

$$nstrs = 1 - \frac{\phi_n}{\phi_n + exp(3.535 - 0.02597 \cdot \phi_n)}, \tag{A3}$$

where ϕ_n is a scaling factor for nitrogen stress computed with the actual and optimal mass of nitrogen stored in the plant material bio_N and $bio_{N,opt}$, respectively:

$$\phi_n = 200 \cdot \left(\frac{bio_N}{bio_{N,opt}} - 0.5\right) \tag{A4}$$

Phosphor stress $pstrs$ is calculated as:

$$pstrs = 1 - \frac{\phi_p}{\phi_n + exp(3.535 - 0.02597 \cdot \phi_p)}, \tag{A5}$$

where ϕ_p is a scaling factor for phosphorous stress computed with the actual and optimal mass of phosphorus stored in the plant material bio_P and $bio_{P,opt}$, respectively:

$$\phi_p = 200 \cdot \left(\frac{bio_P}{bio_{P,opt}} - 0.5\right). \tag{A6}$$

The Kling-Gupta efficiency KGE is calculated as:

$$KGE = 1 - \sqrt{(r-1)^2 + \left(\frac{\sigma_{sim}}{\sigma_{obs}} - 1\right)^2 + \left(\frac{\mu_{sim}}{\mu_{obs}} - 1\right)^2}, \tag{A7}$$

where r is the linear correlation between observations and simulations, σ_{sim} and σ_{obs} are the standard deviation of the simulations and observations, respectively, and μ_{sim} and μ_{obs} are the mean value for the simulations and observation, respectively.

A3 Appendix A3 - Final parameters

Table A1. List of final parameters for the multi-objective (LAI & AET), observed LAI, and GLASS-LAI optimization for the forested region. The units of the parameters are excluded for readability. They are given in Table 2.

Parameter	LAI & AET			Observed LAI			GLASS-LAI			Lower Benchmark		
	HG	PM	PT	HG	PM	PT	HG	PM	PT	HG	PM	PT
BIO_E	26.2	19.5	29.3	20.7	22.2	21.1	18.4	10.3	19.2	36.5	23.3	38.2
BLAI	3.7	4.2	5.5	4.4	4.6	4.8	4.1	5.1	4.6	6.6	2.5	5.8
$FRGRW_1$	0.25	0.14	0.1	0.19	0.12	0.2	0.17	0.1	0.15	0.06	0.26	0.19
$LAIMX_1$	0.26	0.18	0.13	0.22	0.13	0.16	0.21	0.09	0.19	0.08	0.17	0.21
$FRGRW_2$	0.51	0.7	0.81	0.69	0.71	0.73	0.69	0.67	0.73	0.9	0.77	0.74
$LAIMX_2$	0.5	0.72	0.84	0.74	0.72	0.64	0.61	0.61	0.6	0.54	0.64	0.61
DLAI	0.68	0.67	0.7	0.54	0.56	0.55	0.56	0.44	0.6	0.71	0.75	0.52
T_OPT	22.7	29.7	30.2	26.4	29.9	29.6	29.5	31.3	25.3	29.4	27.7	29.4
T_BASE	14	14.6	13	15	15.5	15.2	15.2	15.3	14.1	9.1	17	10.6
ALAI_MIN	0.9	0.76	0.88	0.83	0.8	0.8	0.73	0.61	0.77	0.68	0.48	0.84
GSI	0.006	0.006	0.001	0.004	0.005	0.007	0.004	0.002	0.004	0.003	0.003	0.007
PHU	3696	3962	4427	4140	3940	4074	3872	4361	4109	3176	4007	3165
SOL_D[a]	3381	2914	3148	2729	3195	2980	2727	3295	2680	2754	2696	3415
ESCO	0.52	0.41	0.13	0.55	0.54	0.56	0.48	0.92	0.37	0.14	0.29	0.94
EPCO	0.92	0.32	0.92	0.39	0.39	0.71	0.57	0.79	0.48	0.75	0.23	0.4
CAN_MX	4.3	4.9	0.3	6.4	3.7	3.9	5.7	3.8	5.7	4.9	6.1	7
HRU_SLP	0.022	0.022	0.022	0.022	0.022	0.022	0.022	0.022	0.022	0.022	0.022	0.022
SLSUBBN	91.463	91.463	91.463	91.463	91.463	91.463	91.463	91.463	91.463	91.463	91.463	91.463
CN_2	38	38	38	38	38	38	38	38	38	38	38	38
SOL_AWC[b]	1.82	1.11	1.14	1.35	1.2	1.07	1.27	1.8	1.06	-0.23	0.07	-0.5
SOL_BD[b]	0.04	1.08	-0.38	0.51	1.12	0.74	0.12	0.58	0.33	1.04	1.79	0.36
SOL_CBN[b]	1.85	0.39	0.64	0.58	0.8	1.24	1.07	0.56	0.39	1.48	1.17	1.14
SOL_K[b]	1.43	0.95	1.66	0.91	0.82	0.74	1.25	-0.35	0.48	1.7	0.94	0
SOL_RD	1958	1239	1503	1040	1143	1512	1194	1648	1111	578	1575	1894
GW_REVAP	0.18	0.18	0.18	0.18	0.18	0.18	0.18	0.18	0.18	0.18	0.18	0.18
RCHRG_DP	0.2	0.2	0.2	0.2	0.2	0.2	0.2	0.2	0.2	0.2	0.2	0.2
REVAPMN	500	500	500	500	500	500	500	500	500	500	500	500

[a]Lowest soil layer depth; [b]Relative parameter changes: $para_{new} = para_{original} + para_{original} \cdot para_{change}$

Table A2. List of final parameters for the multi-objective (LAI & AET), observed LAI, and GLASS-LAI optimization for the grassland region. The units of the parameters are excluded for readability. They are given in Table 2

Parameter	LAI & AET			Observed LAI			GLASS-LAI			Lower Benchmark		
	HG	PM	PT	HG	PM	PT	HG	PM	PT	HG	PM	PT
BIO_E	28	18.7	25.4	20.2	23	22.1	19.2	23.5	16.5	23.1	37.6	21.7
BLAI	4.5	4.5	4.4	4.5	4.4	4.7	4.5	5.3	6	4.8	4.9	6.9
$FRGRW_1$	0.29	0.27	0.29	0.3	0.29	0.28	0.24	0.29	0.3	0.07	0.16	0.23
$LAIMX_1$	0.08	0.07	0.06	0.06	0.05	0.05	0.15	0.14	0.14	0.2	0.11	0.15
$FRGRW_2$	0.69	0.67	0.68	0.6	0.61	0.65	0.52	0.56	0.51	0.56	0.59	0.72
$LAIMX_2$	0.72	0.74	0.78	0.74	0.75	0.76	0.75	0.88	0.66	0.61	0.64	0.57
DLAI	0.83	0.83	0.79	0.77	0.8	0.76	0.8	0.59	0.71	0.81	0.88	0.72
T_OPT	30.4	27.8	30.3	29.8	30.5	30.5	20.6	28.6	31.5	28.4	24.5	28.4
T_BASE	12.8	12.9	12.9	13	13	13	11.6	14.4	14.4	11.9	11.1	16.6
ALAI_MIN	0.62	0.6	0.63	0.6	0.61	0.6	0.7	0.65	0.68	0.51	0.26	0.8
GSI	0.005	0.004	0.004	0.005	0.006	0.006	0.008	0.004	0.008	0.001	0.009	0.001
PHU	4090	3970	4010	4087	4035	4059	4104	3843	3535	5638	5665	4571
SOL_D[a]	3002	2541	3375	2883	2911	2967	3866	2390	3575	3392	2270	2835
ESCO	0.89	0.54	0.8	0.49	0.5	0.59	0.49	0.51	0.1	0.28	0.53	0.11
EPCO	0.43	0.27	0.73	0.37	0.52	0.43	0.58	0.15	0.6	0.2	0.87	0.18
CAN_MX	4.3	4.9	0.3	6.4	3.7	3.9	5.7	3.8	5.7	4.9	6.1	7
HRU_SLP	0.032	0.032	0.032	0.032	0.032	0.032	0.032	0.032	0.032	0.032	0.032	0.032
SLSUBBN	91.463	91.463	91.463	91.463	91.463	91.463	91.463	91.463	91.463	91.463	91.463	91.463
CN_2	81	81	81	81	81	81	81	81	81	81	81	81
SOL_AWC[b]	-0.21	-0.4	0.05	0.71	0.43	0.63	-0.17	1.72	0.14	0.1	0.74	1.5
SOL_BD[b]	1.08	0.93	0.98	1.03	0.98	0.93	1.6	1.95	0.48	1	0.5	1.72
SOL_CBN[b]	1.47	1.02	1.59	0.87	1.6	1.07	1.25	1.24	-0.6	0.88	0.28	0.74
SOL_K[b]	0.46	0.61	0.44	0.61	0.7	0.65	0.59	-0.36	1.38	0.13	0.06	-0.06
SOL_RD	1958	1239	1503	1040	1143	1512	1194	1648	1111	578	1575	1894
GW_REVAP	0.18	0.18	0.18	0.18	0.18	0.18	0.18	0.18	0.18	0.18	0.18	0.18
RCHRG_DP	0.2	0.2	0.2	0.2	0.2	0.2	0.2	0.2	0.2	0.2	0.2	0.2
REVAPMN	500	500	500	500	500	500	500	500	500	500	500	500

[a]Lowest soil layer depth; [b]Relative parameter changes: $para_{new} = para_{original} + para_{original} \cdot para_{change}$

A4 Appendix A4 - Water balance components

Table A3. Water balance components for the final runs for the forested region. All quantities listed are in (mm). [1]GW is short for groundwater. The components of the lower benchmark are shown although no calibration was applied.

Model setup	Precipitation	PET	AET	Water yield			Aquifer recharge
				Surface runoff	Lateral flow	GW[1] flow	
PET-HG, Upper BM.	1479.6	1891.1	1098	12.1	16.5	56.2	307.6
PET-HG, LAI-Obs	1479.6	1891.1	1049	7.8	25.6	75.7	373.3
PET-HG, LAI-GLASS	1479.6	1891.1	1060	6.5	14.3	73.5	365.4
PET-HG, Lower BM.	1479.6	1891.1	595.9	18.7	27.2	527.2	836.3
PET-PM, Upper BM.	1479.6	1646.3	969	26.9	82.6	77.4	389
PET-PM, LAI-Obs	1479.6	1646.3	968.9	60.2	90.8	68.1	344
PET-PM, LAI-GLASS	1479.6	1646.3	769.3	78.8	16.3	267.5	593.9
PET-PM, Lower BM.	1479.6	1646.3	626.1	18.6	20.23	511.6	811.9
PET-PT, Upper BM.	1479.6	1392.5	969	20.6	8.2	139.3	444.4
PET-PT, LAI-Obs	1479.6	1392.5	911.4	22.6	36.3	193.3	477
PET-PT, LAI-GLASS	1479.6	1392.5	858.6	11.4	29.1	296.4	556.2
PET-PT, Lower BM.	1479.6	1392.5	572.8	99.7	13.8	533.5	787.2

Table A4. Water balance components for the final runs for the grassland region. All quantities listed are in (mm). [1]GW is short for groundwater. The components of the lower benchmark are shown although no calibration was applied.

Model setup	Precipitation	PET	AET	Water yield			Aquifer recharge
				Surface runoff	Lateral flow	GW[1] flow	
PET-HG, Upper BM.	1424	1809.1	729.7	375.5	12.7	57.4	303.6
PET-HG, LAI-Obs	1424	1809.1	869.8	269.5	19.3	48.4	261.7
PET-HG, LAI-GLASS	1424	1809.1	920	294.6	19.5	34.7	186.4
PET-HG, Lower BM.	1424	1809.1	888.6	291.2	11.1	42.7	230.3
PET-PM, Upper BM.	1424	1623	718.5	331.3	12.8	68.8	358.8
PET-PM, LAI-Obs	1424	1623	899.7	244.8	19.4	47.6	253.5
PET-PM, LAI-GLASS	1424	1623	789	300.8	12	57.8	313.4
PET-PM, Lower BM.	1424	1623	824.5	288	15	55	294.5
PET-PT, Upper BM.	1424	1475.6	751.1	382.1	17.8	50.3	269.5
PET-PT, LAI-Obs	1424	1475.6	786.3	309.8	19.8	56.1	302.3
PET-PT, LAI-GLASS	1424	1475.6	883.4	331.8	25.5	33.2	179
PET-PT, Lower BM.	1424	1475.6	874.6	294.1	13.5	43.2	239.1

A5 Appendix A5 - References of the study site map

Table A5. Overview of the data use for the study site map.

Data	Database name or source
Topography	Copernicus GLO-30 (Copernicus, 2022)
Land use map	Copernicus Global Land Service (Buchhorn et al., 2020)
Water bodies	ArcGIS Pro 2.7.3 (ESRI)
Countries and cities	ArcGIS Pro 2.7.3 (ESRI)
Study site locations	Mamadou et al. (2016)
Catchment extents	Derived with ArcGIS Pro 2.7.3 (ESRI)

Author contributions. FM, TS, FA, YT, JMC, MD reviewed and edited the manuscript; FM, TS, YT, FA, MD conceived and designed the study; FM, FA, JMC acquired the data; FM, TS performed the data analysis and model development and simulations; FM, TS, FA, YT, JMC, MD evaluated the simulations and models. FM wrote the manuscript draft.

Competing interests. The authors declare that they have no conflict of interest.

Acknowledgements. The authors want to thank the BMBF ("Bundesministerium für Bildung und Forschung") for the funding of the FURIFLOOD research project ("Current and future risks of urban and rural flooding in West Africa", Grant No.: 01LG2086B). We would like to thank our partners involved in the FURIFLOOD project for their support. This work was further supported by the European Union's Horizon Europe research and innovation program as part of the UAWOS project ("Unmanned Airborne Water Observing System", Grant Agreement No.: 101081783). We would also like to thank the team of the AMMA-CATCH network for their support and their quick responses in case of any queries.

References

Abbas, S. A., Bailey, R. T., White, J. T., Arnold, J. G., White, M. J., Čerkasova, N., and Gao, J.: A framework for parameter estimation, sensitivity analysis, and uncertainty analysis for holistic hydrologic modeling using SWAT+, Hydrology and Earth System Sciences, 28, 21–48, https://doi.org/10.5194/hess-28-21-2024, 2024.

Abitew, T. A., Arnold, J., Jeong, J., Jones, A., and Srinivasan, R.: Innovative approach to prognostic plant growth modeling in SWAT+ for forest and perennial vegetation in tropical and Sub-Tropical climates, Journal of Hydrology X, 20, 100 156, https://doi.org/10.1016/j.hydroa.2023.100156, 2023.

Ago, E. E., Agbossou, E. K., Galle, S., Cohard, J.-M., Heinesch, B., and Aubinet, M.: Long term observations of carbon dioxide exchange over cultivated savanna under a Sudanian climate in Benin (West Africa), Agricultural and Forest Meteorology, 197, 13–25, https://doi.org/10.1016/j.agrformet.2014.06.005, 2014.

Ago, E. E., Agbossou, E. K., Cohard, J.-M., Galle, S., and Aubinet, M.: Response of CO2 fluxes and productivity to water availability in two contrasting ecosystems in northern Benin (West Africa), Annals of Forest Science, 73, 483–500, https://doi.org/10.1007/s13595-016-0542-9, 2016.

Akoko, G., Le, T. H., Gomi, T., and Kato, T.: A Review of SWAT Model Application in Africa, Water, 13, 1313, https://doi.org/10.3390/w13091313, 2021.

Alemayehu, T., van Griensven, A., Woldegiorgis, B. T., and Bauwens, W.: An improved SWAT vegetation growth module and its evaluation for four tropical ecosystems, Hydrology and Earth System Sciences, 21, 4449–4467, https://doi.org/10.5194/hess-21-4449-2017, 2017.

Archibald, J. A. and Walter, M. T.: Do Energy–Based PET Models Require More Input Data than Temperature–Based Models? — An Evaluation at Four Humid FluxNet Sites, Journal of the American Water Resources Association, 50, 497–508, https://doi.org/10.1111/jawr.12137, 2014.

Arnold, J. G. and Fohrer, N.: SWAT2000: current capabilities and research opportunities in applied watershed modelling, Hydrological Processes, 19, 563–572, https://doi.org/10.1002/hyp.5611, 2005.

Arnold, J. G., Srinivasan, R., Muttiah, R. S., and Williams, J. R.: LARGE AREA HYDROLOGIC MODELING AND ASSESSMENT PART I: MODEL DEVELOPMENT, Journal of the American Water Resources Association, 34, 73–89, https://doi.org/10.1111/j.1752-1688.1998.tb05961.x, 1998.

Atkinson, P. M., Jeganathan, C., Dash, J., and Atzberger, C.: Inter-comparison of four models for smoothing satellite sensor time-series data to estimate vegetation phenology, Remote Sensing of Environment, 123, 400–417, https://doi.org/10.1016/j.rse.2012.04.001, 2012.

Bennour, A., Jia, L., Menenti, M., Zheng, C., Zeng, Y., Asenso Barnieh, B., and Jiang, M.: Calibration and Validation of SWAT Model by Using Hydrological Remote Sensing Observables in the Lake Chad Basin, Remote Sensing, 14, 1511, https://doi.org/10.3390/rs14061511, 2022.

Bliefernicht, J., Waongo, M., Salack, S., Seidel, J., Laux, P., and Kunstmann, H.: Quality and Value of Seasonal Precipitation Forecasts Issued by the West African Regional Climate Outlook Forum, Journal of Applied Meteorology and Climatology, 58, 621–642, https://doi.org/10.1175/JAMC-D-18-0066.1, 2019.

Bossa, A., Diekkrüger, B., and Agbossou, E.: Scenario-Based Impacts of Land Use and Climate Change on Land and Water Degradation from the Meso to Regional Scale, Water, 6, 3152–3181, https://doi.org/10.3390/w6103152, 2014.

Bossa, A. Y., Diekkrüger, B., Igué, A. M., and Gaiser, T.: Analyzing the effects of different soil databases on modeling of hydrological processes and sediment yield in Benin (West Africa), Geoderma, 173-174, 61–74, https://doi.org/10.1016/j.geoderma.2012.01.012, 2012.

Bright, R. M., Miralles, D. G., Poyatos, R., and Eisner, S.: Simple Models Outperform More Complex Big-Leaf Models of Daily Transpiration in Forested Biomes, Geophysical Research Letters, 49, e2022GL100 100, https://doi.org/10.1029/2022GL100100, 2022.

Buchhorn, M., Smets, B., Bertels, L., de Roo, B., Lesiv, M., Tsendbazar, N., Li, L., and Tarko, A.: Copernicus Global Land Service: Land Cover 100m: version 3 Globe 2015-2019: Product User Manual, https://doi.org/10.5281/zenodo.3938963, 2020.

Campolongo, F., Cariboni, J., and Saltelli, A.: An effective screening design for sensitivity analysis of large models, Environmental Modelling & Software, 22, 1509–1518, https://doi.org/10.1016/j.envsoft.2006.10.004, 2007.

Chen, B., Black, T. A., Coops, N. C., Hilker, T., Trofymow, J. A., and Morgenstern, K.: Assessing Tower Flux Footprint Climatology and Scaling Between Remotely Sensed and Eddy Covariance Measurements, Boundary-Layer Meteorology, 130, 137–167, https://doi.org/10.1007/s10546-008-9339-1, 2009.

Chiogna, G., Marcolini, G., Engel, M., and Wohlmuth, B.: Sensitivity analysis in the wavelet domain: a comparison study, Stochastic Environmental Research and Risk Assessment, 38, 1669–1684, https://doi.org/10.1007/s00477-023-02654-3, 2024.

Chu, H., Luo, X., Ouyang, Z., Chan, W. S., Dengel, S., Biraud, S. C., Torn, M. S., Metzger, S., Kumar, J., Arain, M. A., Arkebauer, T. J., Baldocchi, D., Bernacchi, C., Billesbach, D., Black, T. A., Blanken, P. D., Bohrer, G., Bracho, R., Brown, S., Brunsell, N. A., Chen, J., Chen, X., Clark, K., Desai, A. R., Duman, T., Durden, D., Fares, S., Forbrich, I., Gamon, J. A., Gough, C. M., Griffis, T., Helbig, M., Hollinger, D., Humphreys, E., Ikawa, H., Iwata, H., Ju, Y., Knowles, J. F., Knox, S. H., Kobayashi, H., Kolb, T., Law, B., Lee, X., Litvak, M., Liu, H., Munger, J. W., Noormets, A., Novick, K., Oberbauer, S. F., Oechel, W., Oikawa, P., Papuga, S. A., Pendall, E., Prajapati, P., Prueger, J., Quinton, W. L., Richardson, A. D., Russell, E. S., Scott, R. L., Starr, G., Staebler, R., Stoy, P. C., Stuart-Haëntjens, E., Sonnentag, O., Sullivan, R. C., Suyker, A., Ueyama, M., Vargas, R., Wood, J. D., and Zona, D.: Representativeness of Eddy-Covariance flux footprints for areas surrounding AmeriFlux sites, Agricultural and Forest Meteorology, 301-302, 108 350, https://doi.org/10.1016/j.agrformet.2021.108350, 2021.

Copernicus: Copernicus DEM, https://doi.org/10.5270/ESA-c5d3d65, 2022.

Danvi, A., Giertz, S., Zwart, S. J., and Diekkrüger, B.: Comparing water quantity and quality in three inland valley watersheds with different levels of agricultural development in central Benin, Agricultural Water Management, 192, 257–270, https://doi.org/10.1016/j.agwat.2017.07.017, 2017.

Duan, Q., Sorooshian, S., and Gupta, V. K.: Optimal use of the SCE-UA global optimization method for calibrating watershed models, Journal of Hydrology, 158, 265–284, https://doi.org/10.1016/0022-1694(94)90057-4, 1994.

Duku, C., Rathjens, H., Zwart, S. J., and Hein, L.: Towards ecosystem accounting: a comprehensive approach to modelling multiple hydrological ecosystem services, Hydrology and Earth System Sciences, 19, 4377–4396, https://doi.org/10.5194/hess-19-4377-2015, 2015.

Duku, C., Zwart, S. J., and Hein, L.: Modelling the forest and woodland-irrigation nexus in tropical Africa: A case study in Benin, Agriculture, Ecosystems & Environment, 230, 105–115, https://doi.org/10.1016/j.agee.2016.06.001, 2016.

Duku, C., Zwart, S. J., and Hein, L.: Impacts of climate change on cropping patterns in a tropical, sub-humid watershed, PloS one, 13, https://doi.org/10.1371/journal.pone.0192642, 2018.

Fang, H., Baret, F., Plummer, S., and Schaepman-Strub, G.: An Overview of Global Leaf Area Index (LAI): Methods, Products, Validation, and Applications, Reviews of Geophysics, 57, 739–799, https://doi.org/10.1029/2018RG000608, 2019.

Fernandez-Palomino, C. A., Hattermann, F. F., Krysanova, V., Vega-Jácome, F., and Bronstert, A.: Towards a more consistent eco-hydrological modelling through multi-objective calibration: a case study in the Andean Vilcanota River basin, Peru, Hydrological Sciences Journal, 66, 59–74, https://doi.org/10.1080/02626667.2020.1846740, 2021.

Ferreira, A. d. N., de Almeida, A., Koide, S., Minoti, R. T., and de Siqueira, M. B. B.: Evaluation of Evapotranspiration in Brazilian Cerrado Biome Simulated with the SWAT Model, Water, 13, 2037, https://doi.org/10.3390/w13152037, 2021.

Friend, A. D., Arneth, A., Kiang, N. Y., Lomas, M., Ogée, J., Rödenbeck, C., Running, S. W., Santaren, J.-D., Sitch, S., Viovy, N., Woodward, I. F., and Zaehle, S.: FLUXNET and modelling the global carbon cycle, Global Change Biology, 13, 610–633, https://doi.org/10.1111/j.1365-2486.2006.01223.x, 2007.

Galle, S., Grippa, M., Peugeot, C., Moussa, I. B., Cappelaere, B., Demarty, J., Mougin, E., Panthou, G., Adjomayi, P., Agbossou, E. K., Ba, A., Boucher, M., Cohard, J.-M., Descloitres, M., Descroix, L., Diawara, M., Dossou, M., Favreau, G., Gangneron, F., Gosset, M., Hector, B., Hiernaux, P., Issoufou, B.-A., Kergoat, L., Lawin, E., Lebel, T., Legchenko, A., Abdou, M. M., Malam-Issa, O., Mamadou, O., Nazoumou, Y., Pellarin, T., Quantin, G., Sambou, B., Seghieri, J., Séguis, L., Vandervaere, J.-P., Vischel, T., Vouillamoz, J.-M., Zannou, A., Afouda, S., Alhassane, A., Arjounin, M., Barral, H., Biron, R., Cazenave, F., Chaffard, V., Chazarin, J.-P., Guyard, H., Koné, A., Mainassara, I., Mamane, A., Oi, M., Ouani, T., Soumaguel, N., Wubda, M., Ago, E. E., Alle, I. C., Allies, A., Arpin-Pont, F., Awessou, B., Cassé, C., Charvet, G., Dardel, C., Depeyre, A., Diallo, F. B., Do, T., Fatras, C., Frappart, F., Gal, L., Gascon, T., Gibon, F., Guiro, I., Ingatan, A., Kempf, J., Kotchoni, D., Lawson, F., Leauthaud, C., Louvet, S., Mason, E., Nguyen, C. C., Perrimond, B., Pierre, C., Richard, A., Robert, E., Román-Cascón, C., Velluet, C., and Wilcox, C.: AMMA–CATCH, a Critical Zone Observatory in West Africa Monitoring a Region in Transition, Vadose Zone Journal, 17, 1–24, https://doi.org/10.2136/vzj2018.03.0062, 2018.

Garcia Sanchez, D., Lacarrière, B., Musy, M., and Bourges, B.: Application of sensitivity analysis in building energy simulations: Combining first- and second-order elementary effects methods, Energy and Buildings, 68, 741–750, https://doi.org/10.1016/j.enbuild.2012.08.048, 2014.

Gerten, D., Schaphoff, S., Haberlandt, U., Lucht, W., and Sitch, S.: Terrestrial vegetation and water balance—hydrological evaluation of a dynamic global vegetation model, Journal of Hydrology, 286, 249–270, https://doi.org/10.1016/j.jhydrol.2003.09.029, 2004.

Giertz, S. and Diekkrüger, B.: Analysis of the hydrological processes in a small headwater catchment in Benin (West Africa), Physics and Chemistry of the Earth, Parts A/B/C, 28, 1333–1341, https://doi.org/10.1016/j.pce.2003.09.009, 2003.

Giertz, S., Diekkrüger, B., Jaeger, A., and Schopp, M.: An interdisciplinary scenario analysis to assess the water availability and water consumption in the Upper Ouémé catchment in Benin, Advances in Geosciences, 9, 3–13, https://doi.org/10.5194/adgeo-9-3-2006, 2006.

Good, S. P., Soderberg, K., Guan, K., King, E. G., Scanlon, T. M., and Caylor, K. K.: d2 H isotopic flux partitioning of evapotranspiration over a grass field following a water pulse and subsequent dry down, Water Resources Research, 50, 1410–1432, https://doi.org/10.1002/2013WR014333, 2014.

Ha, L., Bastiaanssen, W., van Griensven, A., van Dijk, A., and Senay, G.: Calibration of Spatially Distributed Hydrological Processes and Model Parameters in SWAT Using Remote Sensing Data and an Auto-Calibration Procedure: A Case Study in a Vietnamese River Basin, Water, 10, 212, https://doi.org/10.3390/w10020212, 2018.

Haas, H., Reaver, N. G. F., Karki, R., Kalin, L., Srivastava, P., Kaplan, D. A., and Gonzalez-Benecke, C.: Improving the representation of forests in hydrological models, The Science of the total environment, 812, 151 425, https://doi.org/10.1016/j.scitotenv.2021.151425, 2022.

Hargreaves, G. H. and Samani, Z. A.: Reference Crop Evapotranspiration from Temperature, Applied Engineering in Agriculture, 1, 96–99, https://doi.org/10.13031/2013.26773, 1985.

Hector, B., Cohard, J.-M., Séguis, L., Galle, S., and Peugeot, C.: Hydrological functioning of western African inland valleys explored with a critical zone model, Hydrology and Earth System Sciences, 22, 5867–5888, https://doi.org/10.5194/hess-22-5867-2018, 2018.

Houska, T., Kraft, P., Chamorro-Chavez, A., and Breuer, L.: SPOTting Model Parameters Using a Ready-Made Python Package, PloS one, 10, https://doi.org/10.1371/journal.pone.0145180, 2015.

Hoyos, N., Correa-Metrio, A., Jepsen, S. M., Wemple, B., Valencia, S., Marsik, M., Doria, R., Escobar, J., Restrepo, J. C., and Velez, M. I.: Modeling Streamflow Response to Persistent Drought in a Coastal Tropical Mountainous Watershed, Sierra Nevada De Santa Marta, Colombia, Water, 11, 94, https://doi.org/10.3390/w11010094, 2019.

Jepsen, S. M., Harmon, T. C., and Guan, B.: Analyzing the Suitability of Remotely Sensed ET for Calibrating a Watershed Model of a Mediterranean Montane Forest, Remote Sensing, 13, 1258, https://doi.org/10.3390/rs13071258, 2021.

Jolly, W. M. and Running, S. W.: Effects of precipitation and soil water potential on drought deciduous phenology in the Kalahari, Global Change Biology, 10, 303–308, https://doi.org/10.1046/j.1365-2486.2003.00701.x, 2004.

Judex, M. and Thamm, H.-P., eds.: Impetus Atlas Benin: Research results 2000 - 2007, University of Bonn, Department of Geography, Bonn, 3rd edition edn., ISBN 978-3-9810311-5-7, 2008.

Karvelis, P.: daviolinplot - beautiful violin and raincloud plots, https://github.com/frank-pk/DataViz/releases/tag/v3.2.3, 2024.

Khanal, S. and Parajuli, P. B.: Sensitivity Analysis and Evaluation of Forest Biomass Production Potential Using SWAT Model, Journal of Sustainable Bioenergy Systems, 04, 136–147, https://doi.org/10.4236/jsbs.2014.42013, 2014.

Kim, J., Hwang, T., Schaaf, C. L., Kljun, N., and Munger, J. W.: Seasonal variation of source contributions to eddy-covariance CO2 measurements in a mixed hardwood-conifer forest, Agricultural and Forest Meteorology, 253-254, 71–83, https://doi.org/10.1016/j.agrformet.2018.02.004, 2018.

Knoben, W. J. M., Freer, J. E., and Woods, R. A.: Technical note: Inherent benchmark or not? Comparing Nash–Sutcliffe and Kling–Gupta efficiency scores, Hydrology and Earth System Sciences, 23, 4323–4331, https://doi.org/10.5194/hess-23-4323-2019, 2019.

Koltsida, E. and Kallioras, A.: Multi-Variable SWAT Model Calibration Using Satellite-Based Evapotranspiration Data and Streamflow, Hydrology, 9, 112, https://doi.org/10.3390/hydrology9070112, 2022.

Liang, S., Zhang, X., Xiao, Z., Cheng, J., Liu, Q., and Zhao, X.: Global LAnd Surface Satellite (GLASS) Products, Springer International Publishing, Cham, ISBN 978-3-319-02587-2, https://doi.org/10.1007/978-3-319-02588-9, 2014.

Liang, S., Cheng, J., Jia, K., Jiang, B., Liu, Q., Xiao, Z., Yao, Y., Yuan, W., Zhang, X., Zhao, X., and Zhou, J.: The Global Land Surface Satellite (GLASS) Product Suite, Bulletin of the American Meteorological Society, 102, E323–E337, https://doi.org/10.1175/BAMS-D-18-0341.1, 2021.

López-Ramírez, S. M., Mayer, A., Sáenz, L., Muñoz-Villers, L. E., Holwerda, F., Looker, N., Schürz, C., Berry, Z. C., Manson, R., Asbjornsen, H., Kolka, R., Geissert, D., and Lezama, C.: A comprehensive calibration and validation of SWAT-T using local datasets, evapotranspiration and streamflow in a tropical montane cloud forest area with permeable substrate in central Veracruz, Mexico, Journal of Hydrology, 603, 126 781, https://doi.org/10.1016/j.jhydrol.2021.126781, 2021.

Mamadou, O., Cohard, J. M., Galle, S., Awanou, C. N., Diedhiou, A., Kounouhewa, B., and Peugeot, C.: Energy fluxes and surface characteristics over a cultivated area in Benin: daily and seasonal dynamics, Hydrology and Earth System Sciences, 18, 893–914, https://doi.org/10.5194/hess-18-893-2014, 2014.

Mamadou, O., Galle, S., Cohard, J.-M., Peugeot, C., Kounouhewa, B., Biron, R., Hector, B., and Zannou, A. B.: Dynamics of water vapor and energy exchanges above two contrasting Sudanian climate ecosystems in Northern Benin (West Africa), Journal of Geophysical Research: Atmospheres, 121, https://doi.org/10.1002/2016JD024749, 2016.

Michel, D., Jiménez, C., Miralles, D. G., Jung, M., Hirschi, M., Ershadi, A., Martens, B., McCabe, M. F., Fisher, J. B., Mu, Q., Seneviratne, S. I., Wood, E. F., and Fernández-Prieto, D.: The WACMOS-ET project – Part 1: Tower-scale evaluation of four remote-sensing-based evapotranspiration algorithms, Hydrology and Earth System Sciences, 20, 803–822, https://doi.org/10.5194/hess-20-803-2016, 2016.

Miralles, D. G., Jiménez, C., Jung, M., Michel, D., Ershadi, A., McCabe, M. F., Hirschi, M., Martens, B., Dolman, A. J., Fisher, J. B., Mu, Q., Seneviratne, S. I., Wood, E. F., and Fernández-Prieto, D.: The WACMOS-ET project – Part 2: Evaluation of global terrestrial evaporation data sets, Hydrology and Earth System Sciences, 20, 823–842, https://doi.org/10.5194/hess-20-823-2016, 2016.

Monteith, J. L.: Evaporation and the environment, Symposia of the Society for Experimental Biology, pp. 205–234, 1965.

Morris, M. D.: Factorial Sampling Plans for Preliminary Computational Experiments, Technometrics, 33, 161–174, https://doi.org/10.1080/00401706.1991.10484804, 1991.

Nantasaksiri, K., Charoen-Amornkitt, P., and Machimura, T.: Land Potential Assessment of Napier Grass Plantation for Power Generation in Thailand Using SWAT Model. Model Validation and Parameter Calibration, Energies, 14, 1326, https://doi.org/10.3390/en14051326, 2021.

Neitsch, S. L., Arnold, J. G., Kiniry, J. R., and Williams, J. R.: Soil & Water Assessment Tool Theoretical Documentation Version 2009, 2011.

Nelder, J. A. and Mead, R.: A Simplex Method for Function Minimization, The Computer Journal, 7, 308–313, https://doi.org/10.1093/COMJNL/7.4.308, 1965.

Novick, K. A., Biederman, J. A., Desai, A. R., Litvak, M. E., Moore, D., Scott, R. L., and Torn, M. S.: The AmeriFlux network: A coalition of the willing, Agricultural and Forest Meteorology, 249, 444–456, https://doi.org/10.1016/j.agrformet.2017.10.009, 2018.

Odusanya, A. E., Mehdi, B., Schürz, C., Oke, A. O., Awokola, O. S., Awomeso, J. A., Adejuwon, J. O., and Schulz, K.: Multi-site calibration and validation of SWAT with satellite-based evapotranspiration in a data-sparse catchment in southwestern Nigeria, Hydrology and Earth System Sciences, 23, 1113–1144, https://doi.org/10.5194/hess-23-1113-2019, 2019.

Odusanya, A. E., Schulz, K., Biao, E. I., Degan, B. A., and Mehdi-Schulz, B.: Evaluating the performance of streamflow simulated by an eco-hydrological model calibrated and validated with global land surface actual evapotranspiration from remote sensing at a catchment scale in West Africa, Journal of Hydrology: Regional Studies, 37, 100 893, https://doi.org/10.1016/j.ejrh.2021.100893, 2021.

Park, J. Y., Ale, S., Teague, W. R., and Dowhower, S. L.: Simulating hydrologic responses to alternate grazing management practices at the ranch and watershed scales, Journal of Soil and Water Conservation, 72, 102–121, https://doi.org/10.2489/jswc.72.2.102, 2017.

Poméon, T., Diekkrüger, B., Springer, A., Kusche, J., and Eicker, A.: Multi-Objective Validation of SWAT for Sparsely-Gauged West African River Basins—A Remote Sensing Approach, Water, 10, 451, https://doi.org/10.3390/w10040451, 2018.

Priestley, C. H. B. and Taylor, R. J.: On the Assessment of Surface Heat Flux and Evaporation Using Large-Scale Parameters, Monthly Weather Review, 100, 81–92, https://doi.org/10.1175/1520-0493(1972)100<0081:OTAOSH>2.3.CO;2, 1972.

Qiao, L., Will, R., Wagner, K., Zhang, T., and Zou, C.: Improvement of evapotranspiration estimates for grasslands in the southern Great Plains: Comparing a biophysical model (SWAT) and remote sensing (MODIS), Journal of Hydrology: Regional Studies, 44, 101 275, https://doi.org/10.1016/j.ejrh.2022.101275, 2022.

Rajib, A., Merwade, V., and Yu, Z.: Rationale and Efficacy of Assimilating Remotely Sensed Potential Evapotranspiration for Reduced Uncertainty of Hydrologic Models, Water Resources Research, 54, 4615–4637, https://doi.org/10.1029/2017WR021147, 2018.

Rodell, M., Beaudoing, H. K., L'Ecuyer, T. S., Olson, W. S., Famiglietti, J. S., Houser, P. R., Adler, R., Bosilovich, M. G., Clayson, C. A., Chambers, D., Clark, E., Fetzer, E. J., Gao, X., Gu, G., Hilburn, K., Huffman, G. J., Lettenmaier, D. P., Liu, W. T., Robertson, F. R., Schlosser, C. A., Sheffield, J., and Wood, E. F.: The Observed State of the Water Cycle in the Early Twenty-First Century, Journal of Climate, 28, 8289–8318, https://doi.org/10.1175/JCLI-D-14-00555.1, 2015.

Rogelis, M. C., Werner, M., Obregón, N., and Wright, N.: Hydrological model assessment for flood early warning in a tropical high mountain basin, https://doi.org/10.5194/hess-2016-30, 2016.

Saltelli, A., Ratto, M., Andres, T., Campolongo, F., Cariboni, J., Gatelli, D., Saisana, M., Tarantola, and Stefano: Global sensitivity analysis: The primer, Wiley, Chichester, West Sussex, ISBN 978-0-470-05997-5, 2008.

Schaefli, B. and Gupta, H. V.: Do Nash values have value?, Hydrological Processes, 21, 2075–2080, https://doi.org/10.1002/hyp.6825, 2007.

Schlesinger, W. H. and Jasechko, S.: Transpiration in the global water cycle, Agricultural and Forest Meteorology, 189-190, 115–117, https://doi.org/10.1016/j.agrformet.2014.01.011, 2014.

Schneider, K., Ketzer, B., Breuer, L., Vaché, K. B., Bernhofer, C., and Frede, H.-G.: Evaluation of evapotranspiration methods for model validation in a semi-arid watershed in northern China, Advances in Geosciences, 11, 37–42, https://doi.org/10.5194/adgeo-11-37-2007, 2007.

Seibert, J., Vis, M. J. P., Lewis, E., and van Meerveld, H. J.: Upper and lower benchmarks in hydrological modelling, Hydrological Processes, 32, 1120–1125, https://doi.org/10.1002/hyp.11476, 2018.

Strauch, M. and Volk, M.: SWAT plant growth modification for improved modeling of perennial vegetation in the tropics, Ecological Modelling, 269, 98–112, https://doi.org/10.1016/j.ecolmodel.2013.08.013, 2013.

Tan, M. L., Gassman, P. W., Yang, X., and Haywood, J.: A review of SWAT applications, performance and future needs for simulation of hydro-climatic extremes, Advances in Water Resources, 143, 103 662, https://doi.org/10.1016/j.advwatres.2020.103662, 2020.

Togbévi, Q. F., Bossa, A. Y., Yira, Y., Preko, K., Sintondji, L. O., and van der Ploeg, M.: A multi-model approach for analysing water balance and water-related ecosystem services in the Ouriyori catchment (Benin), Hydrological Sciences Journal, 65, 2453–2465, https://doi.org/10.1080/02626667.2020.1811286, 2020.

Viovy, N., Arino, O., and Belward, A. S.: The Best Index Slope Extraction (BISE): A method for reducing noise in NDVI time-series, International Journal of Remote Sensing, 13, 1585–1590, https://doi.org/10.1080/01431169208904212, 1992.

Wagener, T., McIntyre, N., Lees, M. J., Wheater, H. S., and Gupta, H. V.: Towards reduced uncertainty in conceptual rainfall–runoff modelling: dynamic identifiability analysis, Hydrological Processes, 17, 455–476, https://doi.org/10.1002/hyp.1135, 2003.

Wang, L., Good, S. P., and Caylor, K. K.: Global synthesis of vegetation control on evapotranspiration partitioning, Geophysical Research Letters, 41, 6753–6757, https://doi.org/10.1002/2014GL061439, 2014.

Weerasinghe, I., Bastiaanssen, W., Mul, M., Jia, L., and van Griensven, A.: Can we trust remote sensing evapotranspiration products over Africa?, Hydrology and Earth System Sciences, 24, 1565–1586, https://doi.org/10.5194/hess-24-1565-2020, 2020.

Wei, Z., Yoshimura, K., Wang, L., Miralles, D. G., Jasechko, S., and Lee, X.: Revisiting the contribution of transpiration to global terrestrial evapotranspiration, Geophysical Research Letters, 44, 2792–2801, https://doi.org/10.1002/2016GL072235, 2017.

Weiss, M., Baret, F., Smith, G. J., Jonckheere, I., and Coppin, P.: Review of methods for in situ leaf area index (LAI) determination, Agricultural and Forest Meteorology, 121, 37–53, https://doi.org/10.1016/j.agrformet.2003.08.001, 2004.

Xiang, X., Ao, T., Xiao, Q., Li, X., Zhou, L., Chen, Y., Bi, Y., and Guo, J.: Parameter Sensitivity Analysis of SWAT Modeling in the Upper Heihe River Basin Using Four Typical Approaches, Applied Sciences, 12, 9862, https://doi.org/10.3390/app12199862, 2022.

Yang, Q. and Zhang, X.: Improving SWAT for simulating water and carbon fluxes of forest ecosystems, The Science of the total environment, 569-570, 1478–1488, https://doi.org/10.1016/j.scitotenv.2016.06.238, 2016.

Yang, Q., Almendinger, J. E., Zhang, X., Huang, M., Chen, X., Leng, G., Zhou, Y., Zhao, K., Asrar, G. R., Srinivasan, R., and Li, X.: Enhancing SWAT simulation of forest ecosystems for water resource assessment: A case study in the St. Croix River basin, Ecological Engineering, 120, 422–431, https://doi.org/10.1016/j.ecoleng.2018.06.020, 2018.

Zhang, H., Wang, B., Liu, D. L., Zhang, M., Leslie, L. M., and Yu, Q.: Using an improved SWAT model to simulate hydrological responses to land use change: A case study of a catchment in tropical Australia, Journal of Hydrology, 585, 124 822, https://doi.org/10.1016/j.jhydrol.2020.124822, 2020.